Naval Research Laboratory

Washington, DC 20375-5320

NRL/MR/6750--02-8649

Photoresist Removal in LAPPS

D. LEONHARDT
S. G. WALTON
D. D. BLACKWELL
D. P. MURPHY
R. F. FERNSLER
R. A. MEGER

Charged Particle Physics Branch
Plasma Physics Division

November 27, 2002

REPORT DOCUMENTATION PAGE

Form Approved
OMB No. 0704-0188

1. REPORT DATE *(DD-MM-YYYY)*	2. REPORT TYPE	3. DATES COVERED *(From - To)*
November 27, 2002	Interim Report	

4. TITLE AND SUBTITLE

Photoresist Removal in LAPPS

5a. CONTRACT NUMBER

5b. GRANT NUMBER

5c. PROGRAM ELEMENT NUMBER

6. AUTHOR(S)

D. Leonhardt, S.G. Walton, D.D. Blackwell, D.P. Murphy, R.F. Fernsler, and R.A. Meger

5d. PROJECT NUMBER
67-7641-A3

5e. TASK NUMBER

5f. WORK UNIT NUMBER

7. PERFORMING ORGANIZATION NAME(S) AND ADDRESS(ES)

Naval Research Laboratory, Code 6750
4555 Overlook Avenue, SW
Washington, DC 20375-5320

8. PERFORMING ORGANIZATION REPORT NUMBER

NRL/MR/6750--02-8649

9. SPONSORING / MONITORING AGENCY NAME(S) AND ADDRESS(ES)

Office of Naval Research
800 North Quincy Street
Arlington VA 22217

10. SPONSOR / MONITOR'S ACRONYM(S)

11. SPONSOR / MONITOR'S REPORT NUMBER(S)

12. DISTRIBUTION / AVAILABILITY STATEMENT

Approved for public release; distribution is unlimited.

13. SUPPLEMENTARY NOTES

14. ABSTRACT

The ability of LAPPS to remove standard semiconductor photoresist (PR) was studied. Both material removal rates ("ashing") and anisotropy ("etching") were determined with respect to various conditions, including gas composition, substrate temperature, plasma duty factor, and substrate RF-induced self-bias level. At room temperature, the removal rate increased linearly with substrate bias, with reasonable anisotropic pattern transfer improving above –50 V self-bias. Little change in material removal was seen as gas composition went from pure oxygen to 80% argon, implying the PR removal mechanism in LAPPS was ion-driven, or more specifically ion-energy driven. Construction and modification details of the equipment and diagnostics used in these experiments are given in detail.

15. SUBJECT TERMS

Large area plasmas; Electron-beam produced plasma; Photoresist etching

16. SECURITY CLASSIFICATION OF:			17. LIMITATION OF ABSTRACT	18. NUMBER OF PAGES	19a. NAME OF RESPONSIBLE PERSON
a. REPORT	b. ABSTRACT	c. THIS PAGE			Darrin Leobhardt
Unclassified	Unclassified	Unclassified	UL	55	19b. TELEPHONE NUMBER *(include area code)* (202) 767-7532

Standard Form 298 (Rev. 8-98)
Prescribed by ANSI Std. Z39.18

CONTENTS

PHOTORESIST REMOVAL IN LAPPS

Abstract

The ability of LAPPS to remove standard semiconductor photoresist (PR) was studied. Both material removal rates ("ashing") and anisotropy ("etching") were determined with respect to various conditions, including gas composition, substrate temperature, plasma duty factor and substrate rf-induced self-bias level. At room temperature, the removal rate increased linearly with substrate bias, with reasonable anisotropic pattern transfer improving above –50 V self-bias. Little change in material removal was seen as gas composition went from pure oxygen to 80% argon, implying the PR removal mechanism in LAPPS was ion-driven, or more specifically ion-energy driven. Construction and modification details of the equipment and diagnostics used in these experiments is given in detail.

1. INTRODUCTION

The Large Area Plasma Processing System (LAPPS) developed at NRL has been studied and discussed experimentally previously (see Reference 1 and Section 2.1). The system uses a sheet electron beam to ionize background gas, which results in high density plasmas with very cold plasma electron distributions and low internal electric fields. In order to apply this plasma source and take advantage of its unique qualities in a material modification application, polymer-type materials which are typically very sensitive to high density plasma environments were chosen for these studies. The goal of this work was to determine the ability and limitations of LAPPS to interact with a substrates and produce reactive gas phase components. The unique character of LAPPS (low fields, gas independent) allowed a more sensitive set of experiments to better understand the mechanisms involved with polymer (standard photoresist in this case) removal and pattern transfer.

Manuscript approved October 29, 2002.

1.1. Terminology

"Photoresist" (PR or 'resist') material is a vital component in the fabrication of semiconductor devices. Typically, photoresist is sold in solid or thick liquid form to allow the user to mix [with solvent] for the desired viscosity or application. There is an ever-increasing variety of these materials, such as PMMA (polymethyl methacrylate), PMGI (polymethyl glutarimide), novolac, etc... all of which have various optical characteristics, sensitivities to UV light and chemical resistances. Real semiconductor applications usually entail multiple layers of various types of photoresist, so it is an integral part of the semiconductor industry. In most cases, it is also a high molecular weight organic polymer, which means that it can be considered a reasonable test material for other chemically similar substrates. Details as to the specific materials used will be discussed as needed in the text.

1.2. Ashing v. Etching

'Ashing' of PR usually refers to cleaning the entire surface of unwanted material with no regard for finesse. In a dry process, the surface is preferably bathed with low energy reactive species and anisotropy is not an issue. Ashing is not necessarily confined to PR, but all organic materials (fingerprints, boogers, animal droppings) which are considered chemically reactive with atomic oxygen. Most semiconductor 'ashers' are specifically designed to produce neutral atomic oxygen only and not ions. The rationale is that ions impinging on a substrate are a somewhat uncontrollable quantity which can in turn cause damage, something a cleaning step should be void of. For instance, Axcelis Technologies' FusionES3(i) plasma asher[2] is optimized to convert all plasma ions into atomic oxygen, through well anodized chamber walls and barriers in front of the wafer. Also, since the goal is complete removal of all organic material, surface reactions can be catalyzed by heating the substrate. The ES3i specifies an ash rate of 5.5 microns/minute with a substrate temperature of 270°C.[i] This is achieved using a remote 1.5 kW microwave discharge at 1.5 torr of O_2 (2 slpm[ii]), forming gas (3% H_2 in N_2; 0.4 slpm) and CF_4 (5 sccm). The non-oxygen containing gases in this recipe are empirically found to

[i] At such high temperatures, the PR is at least softened if not liquid; the purpose is to remove material as quickly as possible.

[ii] Standard liters per minute (slpm) vs. standard cubic centimeters per minute (sccm)

maintain/maximize chamber surface passivation to keep wall recombination to a minimum. Measured uniformity across 300mm wafer[3] is less than 5% deviation both within the wafer and from wafer-to-wafer.

'Etching' refers to a directional, anisotropic removal of material. Therefore it is a more controlled and higher finesse process, driven by plasma ion energetics as well as surface chemistry. Incident ions supply the final energy necessary to drive off volatile surface species while also supplying reactive plasma species. Usually, surface temperatures are kept low enough to prevent isotropic processes from occurring at any appreciable rate. The result is 'low', 'medium' and 'high' ion energy ranges that pertain to specific ion-driven processes. At low ion energies, chemical etching dominates; ion energies are too low to really assist in the desorption of volatile products. At higher ion energies, reactive ion etching takes place – a balance between surface chemical reactions and the stimulation of volatile species is achieved and optimum etching takes place. At yet higher ion energies, sputtering of the material dominates, as the ion energy is too great and the surface chemistry cannot keep up. In semiconductor materials, these ion energy regions shift according to the band gap of the material, which also depends on the bond strength on the crystal lattice.

2. HISTORY

The history of LAPPS began with the Agile Mirror program at NRL. Here the beginning of LAPPS is discussed and a fairly lengthy summary of published literature on PR plasma processing is given.

2.1. Agile Mirror and PR Removal Experiment[4]

In July of 1998, a mock system was constructed to investigate the claim that Agile Mirror, or more generally, electron-beam (e-beam) generated plasmas produced tremendous amounts of reactive neutral species. To test this claim, a 13 cm long hollow cathode was used in a plexiglass chamber fitted with a rotary vane pump and a small set of Helmholtz coils. A 'toaster' was designed to hold and electrically isolate the PR sample as well as define the e-beam profile through a slot in the top of the structure (hence, the 'toaster' label). The sample electrodes were positioned 6 and 10 mm back

from the beam slot edge and wired in parallel, so identical voltages were placed on both. The cathode in this test was run at 2 kV with a 200 μs pulse length and repetition rate of 5 Hz, giving a duty factor of 0.1%. The cathode was run in 50 mtorr of O_2, in a magnetic field of 60 Gauss (G), resulting in a 'high impedance mode'. A PR sample[i] patterned with an aluminum mask was exposed to the plasma for 20 seconds of processing time, or 5 ½ hours of actual lab time. During this run, a dc bias of –50 Volts was applied continuously to the sample stage. The result was that all of the resist was removed, providing a lower limit on the removal rate of 1.7 microns/min. For a less than optimized test, this etch rate is nearly half the rate of a state-of-the-art asher being sold today, making the result somewhat suspect. The fact remains that the PR material was indeed removed, but the process should be further analyzed as to completely rule out other possible mechanisms.

The operation of the cathode was consistent with many of the other cathodes used, even demonstrating an unstable low-impedance mode creeping in as the gas pressure rose above 55 mtorr. However, the confining field for the electron beam was only 60 Gauss. The electron gyroradius, r_e, is given by[5] $2.38 \times [T_e(eV)]^{1/2}/B(G)$ which becomes 1.8 cm for a 2 keV electron. Using the full beam energy here is somewhat unrealistic, but does provide an upper bound on r_e. More accurately, the perpendicular beam energy due to actual scattering events should be used. The change in perpendicular energy is given by $d/dz(mv_\perp^2/2)^2 = - m\, d/dz(v_b)$ where $v_\perp$ is the perpendicular beam velocity, v_b is the initial beam velocity (determined by the cathode voltage), m is the electron mass and z is the direction of beam propagation. This simplifies[6] to $2N\sigma_m\varepsilon_b$ where N is the number of atoms/cm^3, σ_m is the momentum transfer cross section and ε_b is the initial beam energy. Working through this calculation the perpendicular beam velocity turns out to be 34 eV/cm. Assuming a constant beam velocity and constant scattering, after 20 cm the beam has acquired 680 eV of perpendicular energy which results in a $r_e \sim 1$ cm. This value of r_e is still larger than the beam edge-to-sample distances used in the experiment.

Also in this experiment, a dc bias was applied to the sample holder electrodes. The electrodes were wired in parallel so that they both were at equal potentials with the grounded slot and beam dump in close proximity. When a bias voltage was applied, a

[i] "PR sample" refers to a silicon wafer, spin-coated with a few microns of standard photoresist material.

diffuse glow filled the toaster region, with brighter regions near the electrodes, implying a secondary ionization source. (This is somewhat reminiscent of the Langmuir probe cleaning technique where a high voltage is applied to the probe to bombard it with high-energy ions from the localized discharge. The plasma being studied serves as a secondary source for the applied high voltage fields.) Typically, when rf is used to add ion energy, a sheath grows in front of the electrode, not a discharge. These phenomena make it difficult to deconvolve the effects attributed to either plasma source.

In general, it would be reasonable to assume that there were no cathode instabilities during this test. According to Reference [4], this assumption is probably not correct; in fact, the data typically showed instabilities in the cathode operation. These instabilities were typically mode competitions in cathode operation or arcs. Additional plasma instabilities were seen when the dc voltage was increased as well. All of these details together warrant the need of a controlled group of experiments to precisely determine the contributions and attributes of LAPPS for processing applications.

2.2. Literature

The following are a number of applicable literature references on resist removal in various plasma sources. Less applicable references are list in Appendix A.

Steinbrüchel, Curtis, Lehmann, & Widman, "Diagnostics of Low Pressure Oxygen RF Plasmas and the Mechanism for Polymer Etching: A Comparison of Reactive Sputter Etching and Magnetron Sputter Etching," *IEEE Transactions on Plasma Science* **PS-14**, 132 (1986). Concluded that the etching of polymers in low pressure oxygen plasma is an ion enhanced reaction, probably with O_2 as a major reactant. Gave an activation energy of 0.25-0.5 eV for PMMA.

Hartney, Greene, Soane & Hess, "Mechanistic Studies of Oxygen Plasma Etching," *JVST A* **6**, 1692 (1988). Claimed that in the low pressure (20-75 mtorr) regime of oxygen RIE plasmas, etch rates of Novolac polymers correlated most directly with the supply of O_2 to the surface. Similar results were seen in ion beam studies which saw an increase in etch rate with background pressure.

Joubert, Pelletier & Arnal, "The Etching of Polymers in Oxygen-based Plasmas: A Parametric Study," *J. Appl. Phys.* **65**, 5096 (1989). Ruled out O_2 dependence on etch rate, but nearly everything else shows strong dependency.

Carl, Hess & Lieberman, "Kinetics of Photoresist Etching in ECR Plasmas," *J. Appl. Phys.* **68**, 1859 (1990). Claimed etch rate of 1500 nm/min with an ion flux > 15 mA/cm^2 at 1 mtorr and 750 Watts. Investigated angle of substrate with respect to 'plasma stream'; state that atomic O is primary etchant.

Jungensen, Hutton & Taylor, "Resist Etching Kinetics and Pattern Transfer in a Helicon Plasma," *JVST A* **10**, 2542 (1992). Claimed etch rate of 1.3 microns/min at 1-3 mtorr, 2.5 kW (in to 6" diameter chamber) and a –500 V rf-induced dc bias on substrate. At low biases, significant isotropic etching was observed. Tremendous number of 'etching' conditions, although very nonlinear etch rate with bias energy; strong chemical etching in most if not all cases.

Pang, Sung & Ko, "Etching of Photoresist Using Oxygen Plasma Generated by a Multipolar ECR Source," *JVST B* **10**, 1118 (1992). Claimed etch rate of 1.85 microns/min with 5 mtorr, 1 kW ECR and a –150 V biased substrate 3 cm from plasma source. As sample was moved out from source, etch rate dropped linearly; concluded that the etching is enhanced by ions but neutral reactive species are important. Argon/oxygen mixtures showed decrease in etch rate and roughened surface.

Zeuner, Meichsner & Poll, "Oxidative Decompositon of PMMA in Plasma Etching," *Plasma Sources Sci. Technol.* **4**, 406 (1995). Concluded atomic oxygen radicals are essential for oxidative etching while ion bombardment is the energetically dominant activation mechanism. Specifically designed chamber for O atom fluxes.

Collart, Baggerman & Visser, "On the Role of Atomic Oxygen in the Etching of Organic Polymers in an RF Oxygen Discharge," *J. Appl. Phys.* **78**, 47 (1995). Concluded through

LIF measurements that atomic oxygen doesn't play a significant role in the chemical etching of PR. Concluded that ion bombardment was rate limiting step. Addition of CF_4 showed that atomic F plays major role in etching.

Tang, Nichols & Manos, "Stripping and Cleaning of Photoresist Using Low Energy Neutrals," *J. Appl. Phys.* **86**, 2419 (1999). Measured an activation energy for PMMA of 0.4 eV.

Shüppert, Brose, Peterman & Moosburger, "Anisotropic Plasma Etching of Polymers using a Cryo-cooled Resist Mask," *JVST A* **18**, 385 (2000). Had to cool substrate to (–50°C) for anisotropic etching.

Takechi & Leiberman, "Photoresist Etching in an Inductively Coupled, Traveling Wave Driven, Large Area Plasma Source. *J. Appl. Phys.* **89**, 869 (2001). Obtained etch rate of ~ 100 nm/min without substrate bias and unknown surface temperature. Modeled a lot of aspects, but focus on O_2^+. Come up with a volume-averaged model, including atomic oxygen density at substrate. A little hard to follow.

Panda, Economou & Chen, "Anisotropic Etching of Polymer Films by High Energy (~100s of eV) Oxygen Atom Neutral Beams," *JVST A* **19**, 398 (2001). Used ICP to make neutral beam. "High rate of removal" = 0.6 microns/minute. See a square root dependence of etch rate with bias energy. As sample temperature goes from 5 to 90 °C, etch rate is constant; lack of undercutting is attributed to surface charging. Assumed that O and O^+ are the only reactive species.

Standeart, Matsuo, Li, Oehrlein, Lu, Gutmann, Rosenmayer, Bartz, Langan & Entley, "High Density Plasma Patterning of Low Dielectric Constant Polymers: A Comparison Between Polytetrafluoroethylene, Parylene-N and Poly(arylene ether)," *JVST A* **19**, 435 (2001). Anisotropy hard to realize with O_2 etch of polymers. High lateral erosion rate right at hardmask due to atomic and molecular oxygen reflecting from feature bottom; without ion impact, desorption of etch products was concluded to be induced by the UV

light. Proposed mechanism (1) oxygen adsorbs on surface (2) desorption initiated by the impact of energetic ions. Surface oxidation is reduced as ion energy is increased.

3. EXPERIMENTAL SETUP

3.1. Plasma Chamber and Cathode Operation

All experiments were carried out using a brass hollow cathode with straight side-walls surrounded by a ground shield. Telfon sheet insulated the hollow cathode from the ground shield with additional thin strips ("ribs") of teflon located every few inches along the backside to prevent the occurrence of flash-overs. The hollow part of the cathode was cut with a 9.5 mm (3/8") ball mill, approximately 1 cm deep and 30 cm long, then polished to a mirror-like finish. High voltage pulses were provided with a homemade IGBT pulser unit[7] with a 100 μF charging capacitor which was in turn powered by a Peschel Instruments power supply (3kV/4Amps max). A slotted anode was located 5-8 cm in front of the cathode, made from 1/8" thick stainless steel plate and shim stock. The shim stock position was adjusted to provide a 25 cm x 1 cm slot to define the geometric beam shape of the electron beam produced by the cathode. A similar anode, without a slot was located ~ 50 cm away from the slot and acted as a beam dump. Both of the anodes were grounded outside the vacuum chamber so that their currents could be monitored using Pearson coils. The cathode was located 7.5 cm off of the center axis of the chamber and a set of Helmholtz coils (~ 3 Gauss/amp) was wound directly onto the chamber itself. The vacuum chamber was an aluminum cylinder with a 47.5 cm inner diameter. A base vacuum of ~ 5×10^{-7} torr was provided by a 150 l/s turbomolecular pump and gas flow was provided by mass flow controllers and throttling the turbo pump with a manual gate valve. Operating pressures were monitored by a Convectron© gauge and corrected when necessary for the gas.

With magnetic fields of 150-250 G, this hollow cathode operated in a typical 'high impedance' mode as discussed previously.[4,8] Basically during operation, the hollow cathode discharge emulated a 10kΩ load for a 2 kV pulse. Pulse lengths were varied from 0.5 to 5 milliseconds (ms) and repetition rates were adjusted from 2 to 200 Hz. 'Typical' currents as measured by external Pearson coils were ~ 600 mA cathode

current, 300 mA slotted anode current and 200 mA beam dump anode current[9]. See Section 3.3.3 for further information on these measurements.

3.1.1. IGBT unit vs E-tube[10]

In an effort to alleviate intermittent problems with the IGBT (Insulated Gate Bipolar Transistor) pulser unit, an electron tube pulser unit was constructed. Schematic diagrams of both of these units is given in Appendix B. The most significant improvements in the long-term performance of the pulsed hollow cathode system were eventually found to be: (1) careful cleaning and assembly of the cathode itself (2) replacing charging capacitors and current-limiting resistors (see Section 3.1.3) with more robust components and (3) getting a 'good' set of IGBTs for use in pulser unit. Once the IGBT unit and cathode performance were upgraded and performed consistently, the electron tube unit was decommissioned.

Although the electron tube unit seemed to work initially, it was never fully tested until problems were evident. This was unfortunate, as there was no documentation or history available for troubleshooting. The dominant problems were a sensitive trigger signal and a significant intermittent output voltage drop. It was not clear whether this was a faulty component problem with the circuit or a serious design flaw, utilizing under-rated electronic components.

3.1.2. Duty cycle problems

The primary problems with LAPPS performance for resist etching can be tracked back to insufficient pulse energy with increasing duty factor. Specifically, the charging capacitor(s) and current limiting resistors in the pulser unit needed to be replaced for increased power delivery and dissipation, as well as the voltage divider sensor which was in parallel with the cathode. Typical values before these changes[11] for the external readings of cathode-anode voltage ($V_{A\text{-}K}$), cathode current (I_{cath}), slotted anode current (I_{slot}) and the beam dump anode (I_{dump}) are shown in Table I for typical etching conditions (5 ms pulse length, 2 kV applied voltage, 55 mtorr oxygen and a 165 Gauss magnetic field).

Table I External sensor readings prior to component(s) upgrade. Plasma operating conditions are discussed in the text.

REPETITION RATE (Hz)	V_{A-K} (Volts)	I_{cath} (mA)	I_{slot} (mA)	I_{dump} (mA)
0.5	1827	434	192	244
1	2070	379	200	212
5	1827	488	360	139
20	1971	460	392	68

In the next phase of development, a Langmuir probe was inserted in the plasma channel, to compare the plasma density with the external sensor measurements. The charging resistor (R_c) and current-limiting resistor (R_{cl}) had also both been replaced; R_c was changed from 240Ω/50W to 40Ω/570W and R_{cl} went from 50kΩ to 5kΩ. The Langmuir probe was run in ion saturation mode, being held at a fixed bias voltage of –10 V. Probe data was taken width a 1ms pulse length[12] while external sensors measurements were taken at 5 ms pulse lengths,[13] thus data sets are compared in Table II with respect to duty cycle.

Table II In situ probe measurement and ex situ sensor measurements after replacement of R_c and R_{cl}.

DUTY FACTOR (%)	V_{A-K} (Volts)	I_{cath} (mA)	I_{slot} (mA)	I_{dump} (mA)	I_{probe} (μA)
.5	2070	471	171	302	73
1	2052	475	231	256	73
2	2052	475	290	206	73
5	2034	465	336	120	75
10	1953	428	360	82	74
20	1926	383	342	46	72
50	1863	273	246	36	63

There were significant inconsistencies in the measured plasma densities with respect to the ex situ sensor measurements. The measured plasma ion currents varied by only 15%

overall whereas as the other sensors varied by a minimum of 10% (V_{A-K}) and a maximum of 88% (I_{dump}).

3.1.3. Beefing up of charging capacitor

After upgrading the aforementioned resistors, the charging capacitor was also replaced[14] to increase the deliverable power to the hollow cathode. An additional 300μF/3kV capacitor was placed in parallel with the pre-existing charging capacitor. These component upgrades are listed in Table III.

Table III IGBT pulser unit component values

	R_{cl}	R_c	C_s
INITIAL VALUE	240Ω/50W	50kΩ	32μF/5kV
FINAL VALUE	40Ω/570W	5kΩ	332μF/3kV

With the changes listed in Table III, steadier waveforms and cathode operation were seen overall. Graph 1[15] gives a complete set of measurements taken simultaneously referenced to their maximum value, for a constant repetition rate of 10 Hz. All following measurements and experiments have been carried out with the power supplies in this final configuration.

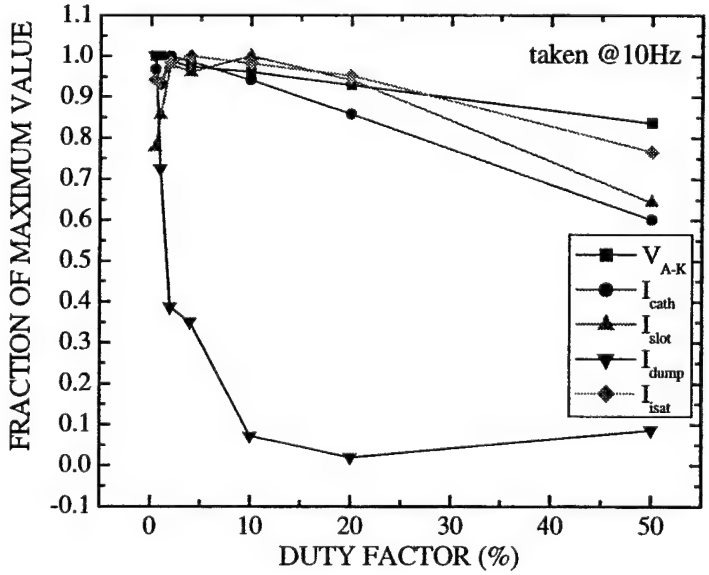

Graph 1 External plasma parameter readings and Langmuir probe saturation current for final configuration of power supply.

3.2. Etching Stage

3.2.1. Design and construction

The etching stages used were constructed from stainless steel, copper and boron nitride. A scaled AutoCad drawing of the assembled stage is shown in Figure 1 and drawings of individual parts is given in Appendix C. The head of the stage was a stainless steel plate (1), which was recessed into the boron nitride insulator (2) approximately 11 cm in diameter. The front plate contained four tapped holes on a 3.8 cm bolt circle to fasten the sample carriage to the stage. This sample carriage was a small stainless steel plate (0.75 mm thick) with slots around the perimeter to accommodate the stage mounting screws, which allowed rapid sample changes (via multiple carriages). Samples were adhered to the carriage with silver print epoxy. This method is typically used to hold samples for scanning electron microscopy (SEM), thus offers good vacuum compatibility and minimal reactivity for these plasma processing studies. The main structural support of the head was provided by two copper[i] plates (3), which housed a 6.4 mm water cooling line (4). The entire head was held together by four 4-40 screws (see detail in figure) which kept the front and back plates electrically isolated with Macor© cups (5), plugs (6) and alumina sleeves (7). The electrical connection to the front plate was provided by a center pin which came up through the assembly and was housed in the stainless steel main support shaft (8). This main support shaft was a 3.2 cm OD stainless steel tube which supported the head and housed all electrical connections, which were fed out through a KF50 vacuum flange at the other end (not shown).

The stage was flange-mounted (ISO160) so that the position of the sample could be adjusted via loosening three Cajon Ultra-torr© fittings (9). Parallelism between the main shaft and water cooling lines was maintained by two identical aluminum clamping blocks (10) located on either side of the mounting flange. To have a relative measurement of the front surface temperature, a K-type thermocouple (not shown) was embedded into the boron nitride piece, close to the front surface. The entire length of stage assembly from front surface to the KF50 electrical feed through flange was 64 cm.

[i] After the initial assembly, one of these copper plates was replaced by an aluminum plate to reduce the mass of the stage front.

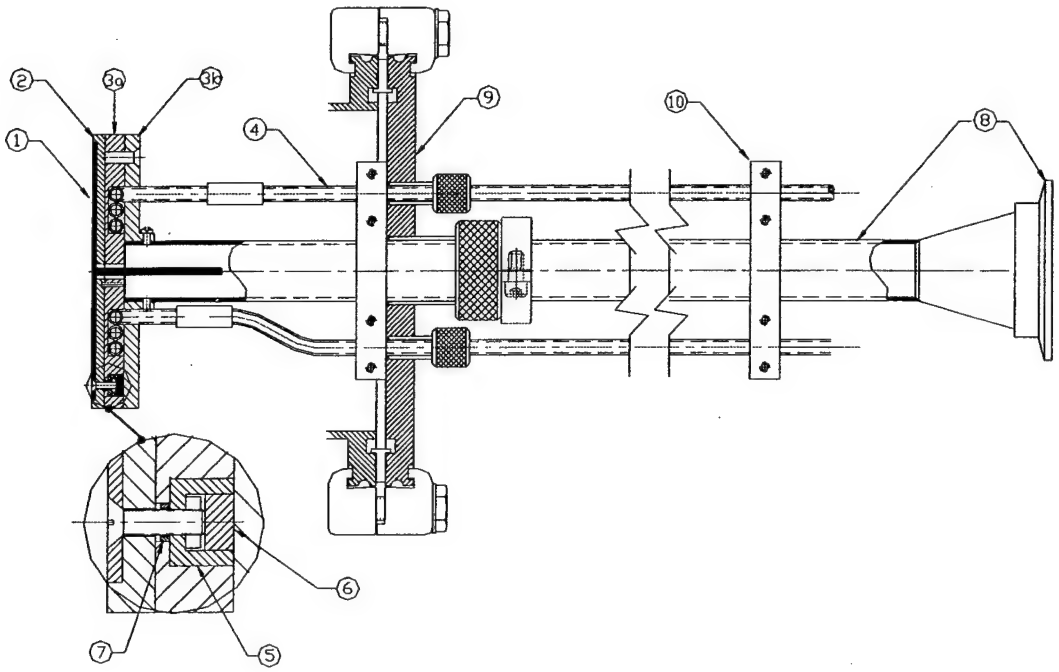

Figure 1 Processing stage drawing; see individual components in Appendix C.

3.2.2. Stage as a probe[16]

The plasma current to the stage was measured under a variety of experimental conditions. In these configurations, the stage is effectively a large planar Langmuir probe, which probably does alter the plasma to some extent. A 'pick-off' box was constructed and mounted directly on the stage feedthrough to alleviate connection inconsistencies and noise introduced by erroneous ground loops. It was constructed from a standard bud box, using standard type N panel mount connectors which mate directly to the stage and laboratory power supplies. The box housed a small (1V/A) Pearson coil which enclosed the main power feed to measure current flow and a standard 10X oscilloscope probe which allowed a consistent reading of the stage voltage. For the measurements discussed in this section, all applied voltages are dc and therefore the stage is indeed a large area probe.

Current flow to the stage was measured in two configurations: with the stage floating (grounded through the 10X probe) and by biasing the stage to negative voltages and measuring the current through a sense resistor during the plasma pulse. All data was

taken at 'standard plasma conditions' (55 mtorr O_2, -2 kV pulse and 165 G magnetic field). In these measurements, the pulse length was fixed at 1 ms and single-point readings were taken at the end of the pulse. As discussed in Section 3.1.3 and shown in Graph 1, the voltage across the plasma sheet remained basically constant in these measurements. The currents measured through the load resistor (I_{LR}) and the Pearson coil (I_{PC}) for the floating stage are in Table IV and with the stage biased at –10 V in Table V. Measured voltages are converted to their ion currents via $I_{measured} = V_{measured}/R_{load}$ where $R_{load} = 10^6\ \Omega$ for 10X probe and 10 Ω for biased stage measurements.

Table IV Current measurements to floating stage.
(Pearson coil showed no measurable currents.)

REPETITION RATE (Hz)	STAGE CURRENT (nA)
1	420
2	439
5	426
10	322
20	182
50	-22

Table V Current measurements to stage biased at –10Vdc.

REPETITION RATE (Hz)	I_{LR} (mA)	I_{PC} (mA)
1	12.4	10.9
2	12.8	10.8
5	12.8	11.1
10	12.8	11.1
20	12.8	10.7
50	12.3	10.6
100	12.1	10.0

From the values given in Table V, we see a reasonable agreement between the two measurements, which when divided by the stage area of 94 cm^2, yields an ion flux density of ~ 130 $\mu A/cm^2$. The temporal responses of these measurements are shown in Graph 2.

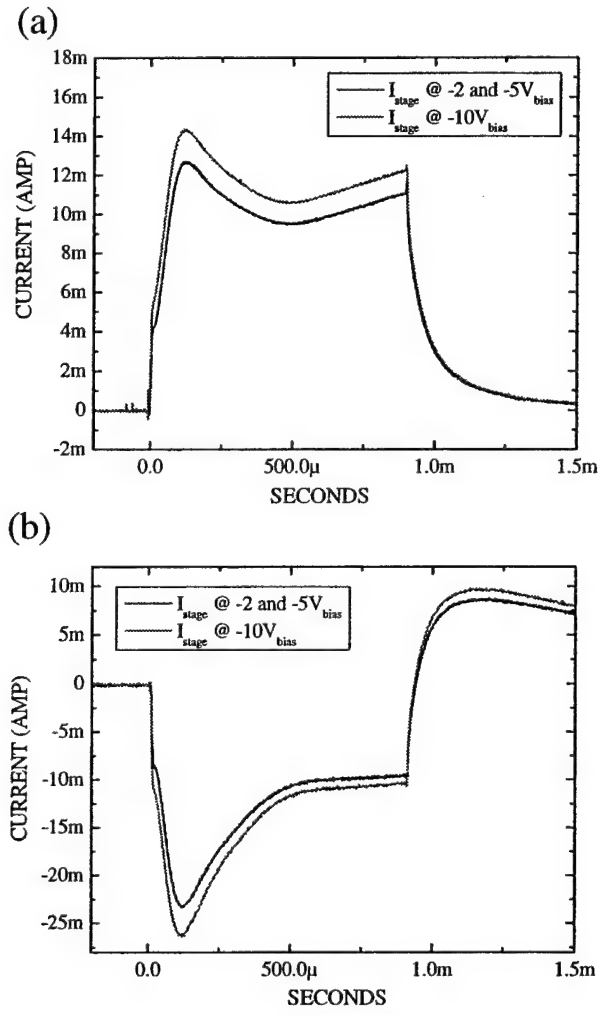

Graph 2 Temporal dependence of stage currents measured through (a) load resistor and (b) Pearson coil at various dc bias levels

3.3. Rf biasing

Applying a capacitively coupled rf signal to the stage induces a negative dc voltage on the stage, as the electrons are able to react to the rf field but not the massive ions.[17] Therefore when an ion does enter the sheath, it is accelerated by a dc electric field into the surface, increasing the directionality and energy of the ion flux. Otherwise, with a

grounded surface, the particle gains approximately $5T_e$ of energy [normal to the surface] as it traverses the sheath. The stage was purposely built to accommodate large rf signals to achieve large dc bias levels. Rf power was applied to the stage through the rf 'pick-off' box discussed in the previous section in series with a commercial capacitive matchbox ('pi' configuration) and rf amplifier powered from a signal generator. In terms of rf power coupled to the stage, the external measurements made in the pick-off box are not necessarily correct but should provide relative values for the rf currents, voltages and rf-induced dc bias ('rfidcb' or just 'rf bias') levels. Ideal matching or coupling of the applied rf voltage to the plasma was considered to be when the rf bias and rf signal amplitude were at a maximum during the beam pulse. Later measurements of forward and reflected rf power (using an inline Bird Electronics directional coupler) showed that indeed the best coupling of the stage to the plasma was achieved at these conditions. The power coupled to the plasma through the stage was > 85%, at these matchbox conditions. Adding an identically sized ground plate symmetrically on the other side of the LAPPS sheet had no effect on rf biasing of the processing stage, and therefore was considered unnecessary for these experiments.

3.3.1. Syncing of rf to plasma pulse[18]

Through the external measurements made at the pick-off box, it was apparent that an rf-driven plasma would continue after the e-beam was turned off. Graph 3 shows an example of this secondary discharge from an oxygen plasma produced by a 500 μs e-beam with the rf voltage applied during the pulse and continued for approximately 1.25 ms afterward.

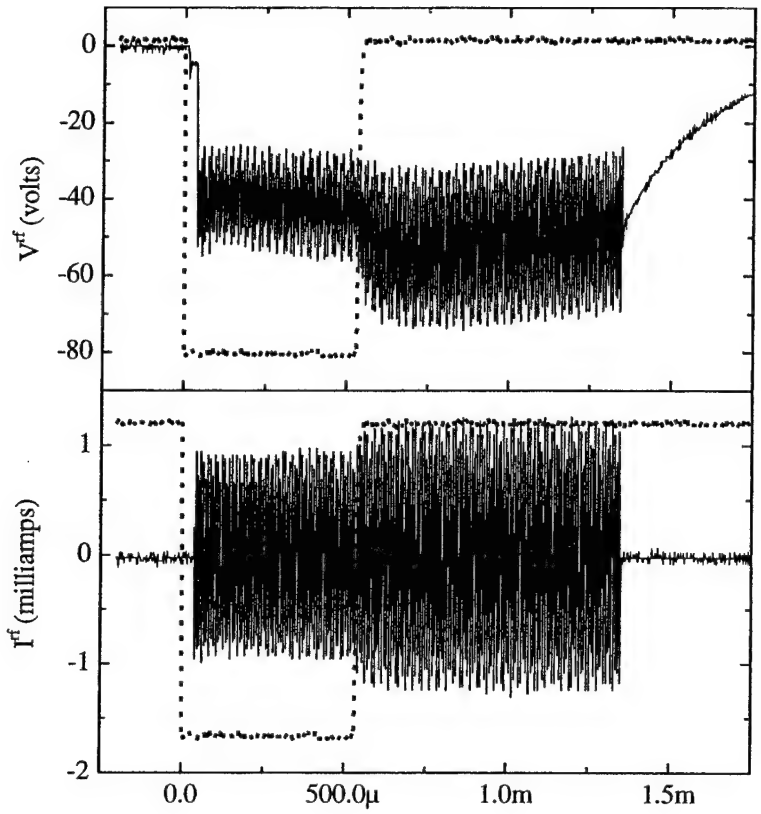

Graph 3 Rf signals measured at pick-off box. Dotted line represents 500µs LAPPS plasma pulse. In 55 mtorr O_2.

For comparison, Graph 4 shows the effect when a significant fraction of SF_6 was added to this plasma. Aside from needing to apply additional rf power to obtain the same dc bias level, the secondary discharge in this case isn't sustained; immediately after the e-beam goes off, the dc level of the voltage drops to zero. No secondary rf discharge could be sustained with the addition of the electronegative gas.

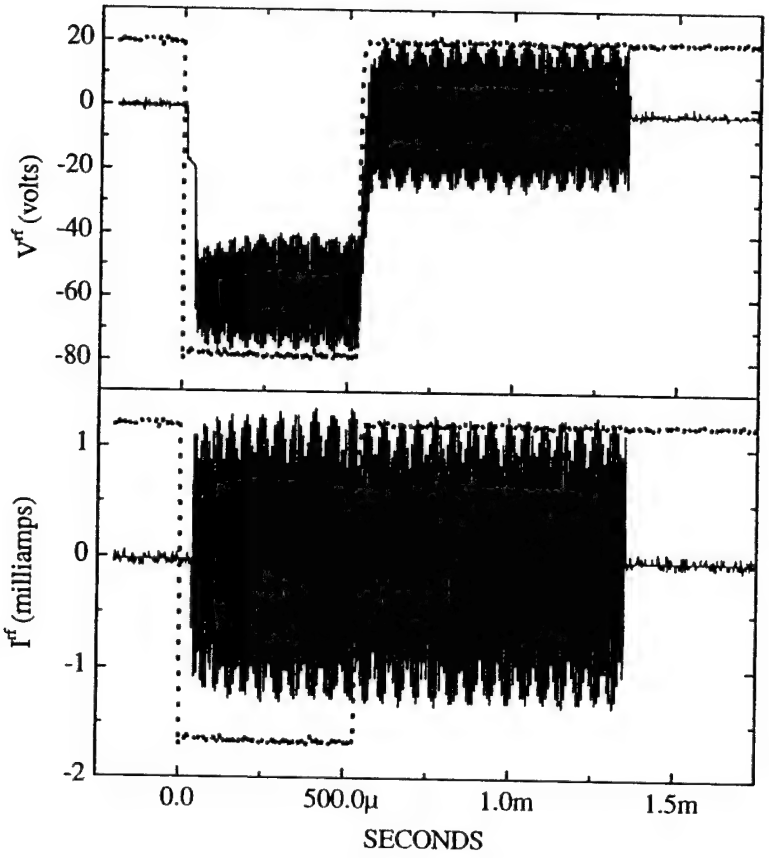

Graph 4 Rf signals measured with ~30% SF_6 in O_2 plasma shown in Graph 3

3.3.2. Addition of shielding around stage[19]

It was found that an additional grounded shield around the perimeter of the stage insulator helped to maintain stable operation of the rf coupling and permitted larger rf bias voltages to be applied to the stage. The ground shield was made from either copper tape or stainless steel shim stock wrapped so that it was flush with the front surface of the stage head. Typically only a 50 V rf bias could be achieved without the additional ground shield. When it was installed around the insulator, stable rf bias levels > 125 V were achieved.

3.3.3. Odd occurrences in standard LAPPS measurements; rf biasing and rf-induced instabilities[20]

When an rf bias was applied to the etching stage, the typical signal levels measured on cathode and anodes showed unexpected dependencies. Specifically, the rf signal was picked up on the cathode current, slotted anode and beam dump monitor, but not on the voltage divider which was in parallel with the plasma. When the electron-tube modulator was used to drive the cathode, a tremendous amount of rf signal and dc level instabilities were observed. When the IGBT modulator was used however, the rf on the cathode current appeared to be merely rf pickup – only an ac signal was seen with no dc component.[i] On both of the anodes however, significant changes were seen in the electron current levels when an rf bias was applied to the etching stage. Graph 5 shows the changes in these current levels when an rf bias is synced to the middle of the e-beam pulse.

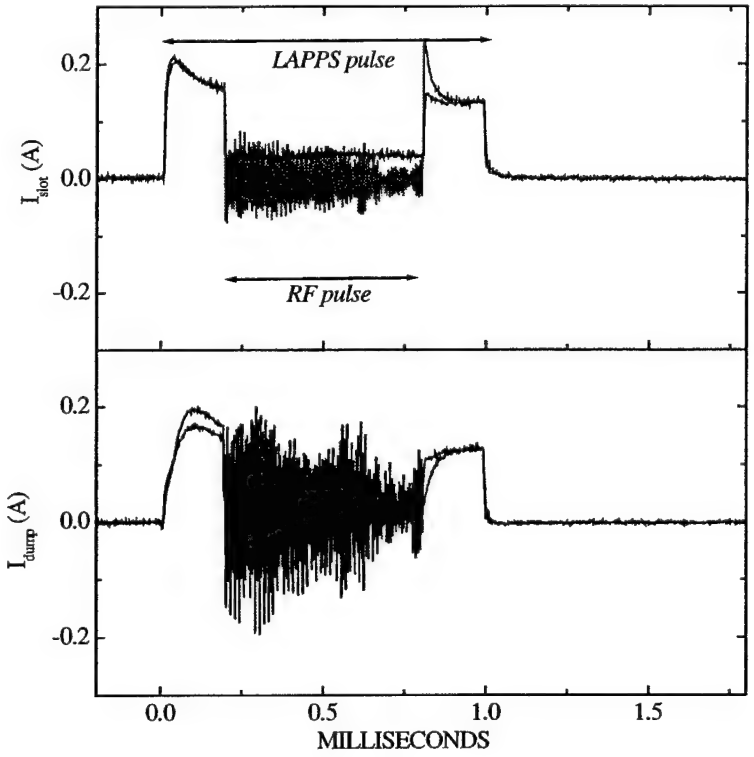

Graph 5 Anode currents when rf is applied to stage. Grey traces are raw signals; black traces are when rf chokes are inserted on the signal line.

[i] After this observation, the e-tube modulator was abandoned for any further materials' processing tests.

These signals are from an O_2 plasma operating at 1.5 kV with a 100 V peak-to-peak rf voltage applied to stage. The 'structure' of the rf envelope is due to the mismatch between oscilloscope time scale resolution and the high frequency (~13.6 MHz) rf signal, which resulted in odd beat patterns which should be ignored. From the data in Graph 5, a significant decrease was seen in the detected electron currents to both anodes. Inserting rf chokes removed the high frequency components (black) from the raw data (grey) but the dc levels induced by the rf signal on the stage remained. In the absence of an e-beam produced plasma, no measurable rf signals were seen on the anodes.

3.3.4. Typical etching conditions

As mentioned previously, 'standard' etching condition were set by: the cathode operating at a 10% duty factor with a –2 kV pulse in a 165 G magnetic field; 55 mtorr O_2 (see Section 4.3 about flow rates); the sample located 8 mm from the beam edge defined by the slotted anode; a -50 V bias on stage. All etch rates were determined by SEM analysis. In order to minimize any effects from undesired discharges, the rf signal was only applied during the e-beam pulse. In this way, the results can be considered to be well correlated to the e-beam produced plasma.

Typical rf biasing was achieved by tuning the rf matchbox and increasing the rf amplitude until a desired dc offset was obtained. This was usually straightforward, and resulted in a peak-to-peak (p-p) rf voltage that was nearly twice the de bias level. The measured rf currents showed a small dc levels[i] (a few mA) and large p-p values (multiple amps). Table VI shows these values for various rf bias levels.[21] When LAPPS was not on, average dc bias levels on the stage were very small (and even positive) while the p-p values would follow a linear V = IR relationship where R ~ 50 Ω. When $V_{p\text{-}p} > 130$ V, significant increases in dc signal levels arose, presumably due to an independent rf-driven discharge around the stage.

[i] Measurements of mean rf currents were skewed by oscilloscope resolution when p-p amplitude became large. Because of these erroneous readings, any further data has been omitted.

Table VI Rf bias measurements when coupled to LAPPS. Average rf current values were typically in the 1-5 mA range.

V_{mean}(V)	V_{p-p}(V)	I_{p-p}(A)
-50	90	1.32
-100	184	2.42
-150	280	3.67
-203	390	5.25
-250	487	6.88
-300	597	8.80

3.4. Samples

A number of different resist samples were tried in these studies. It quickly became evident that a mask in good contact with the surface was necessary to reliably look at issues of anisotropy. Simple masks consisting of macroscopic wires or metal clips did not provide adequate surface contact to look at undercutting at the mask.

3.4.1. Metal masked samples

Chromium-masked resist samples were prepared by the NRL Nanofabrication Facility. Sample patterns of 5-100 μm features were made by a negative/positive resist technique where the bottom (negative) resist is insensitive to the top (positive) resist

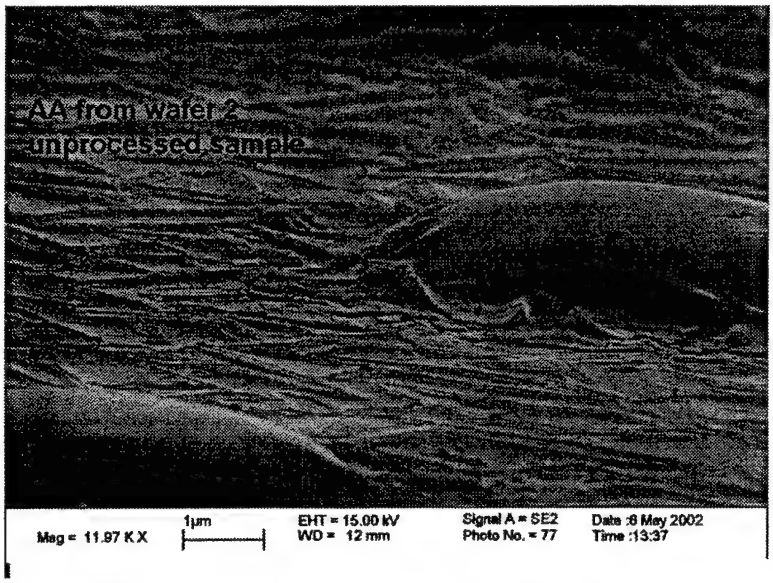

Figure 2 Unprocessed sample showing 5μm 'dot' of chromium mask on blanket of negative photoresist.

developing processes and is therefore patterned like a bulk wafer. Due to the non-conducting nature of resist, it was necessary to gold coat (~10 nm) the samples to produce reasonable SEM images. SEM images of an unprocessed sample is shown in Figure 2.

3.4.2. To rinse or not to rinse

The semiconductor industry has not been able to get away from using a water rinse after a standard ashing process. It had been observed in these experiments that surfaces of processed samples had cotton-like residues when they were not rinsed and these residues were noticeably less after a simple water rinse. Figure 3 compares a rinsed (top) and not rinsed (bottom) sample after undergoing the same etch process. Note the heavy debris on the open area on the bottom picture. All samples were subsequently rinsed.

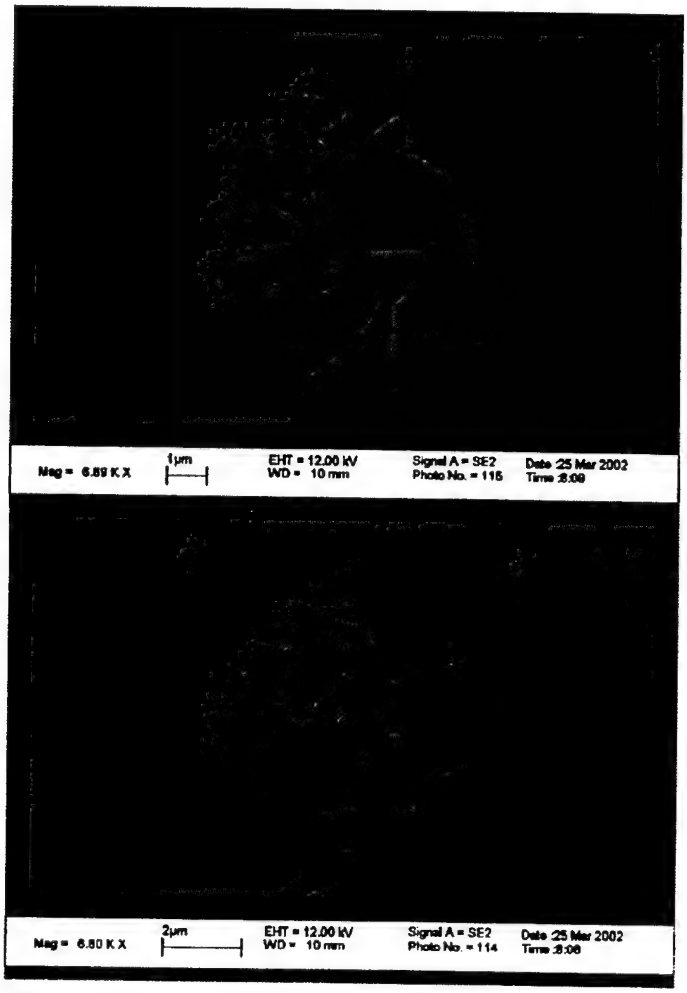

Figure 3 SEM images of samples which have (top) and have not (bottom) undergone a post-process H_2O rinse after a –50 V etching process.

4. ETCHING DATA

A listing of all individual etches with all experimental setting and readings is given in Appendix D, in an Excel spreadsheet format.

4.1. Etch rate with respect to rf bias

The variation of etch rate (ER) with respect to the rf bias level is shown in Graph 6. For ion energies above 50 eV, the mask became fractured as was shown in Figure 3. A moderately linear relationship between ion energy and ER was seen, although at higher voltages the ER started to increase more strongly.

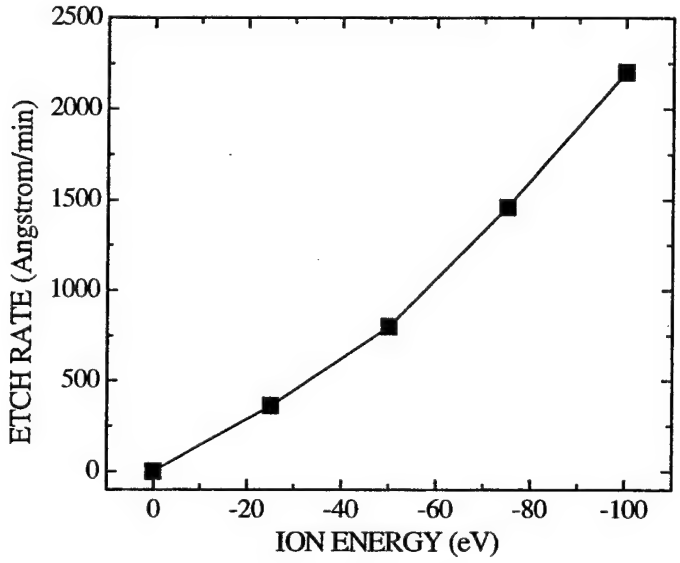

Graph 6 ER of negative resist material versus ion energy

When ion energies were below 50 eV, strong undercutting at the mask-resist interface was seen in the patterned samples. Very anisotropic feature profiles evolved when the ion energy was increased above 50 eV, although truly vertical profiles weren't seen until approximately 100 eV. Although the higher ion energy increased feature anisotropy, damage was also incurred on the surface of the organic material. These effects were most dramatically seen when previously [industrially] ashed via[i] structures were etched in LAPPS to remove ash process residues left in the vias. Figure 4[22] show

[i] Vias are small patterned holes in a substrate, on the order of hundreds of nanometers in diameter.

SEM photos of via structures before etching in LAPPS (top) after a 50 eV etch (middle) and after a 100 eV etch bottom.

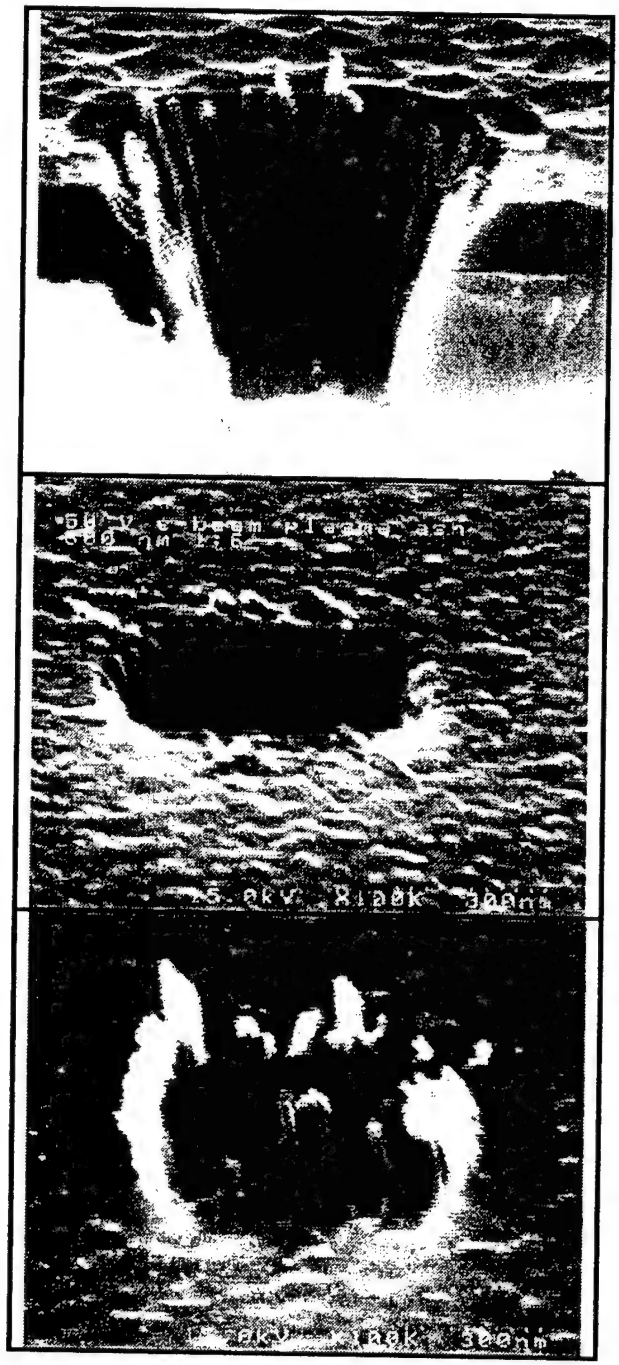

Figure 4 Copper masked via structures before LAPPS etch (top); after –50 V bias etch (middle); and after –100 V bias etch (bottom).

At 50 eV ion energies, the residues left behind by the commercial ashing process were almost completely removed. When the ion energy was increased to 100 eV, growths from the inner walls of the structure are seen, presumably from graphitization of the resist material due to excess energy deposition to surface species.

4.2. Etch rate with respect to duty cycle and gas flow rate[23]

No effect in ER was seen as the duty cycle of the plasma was varied from 0.5% to 50% while keeping the total plasma exposure time constant. Similarly, as gas flow was increased from 6 to 80 sccm, no increase in ER or surface quality was seen.

4.3. Etch rate with respect to gas mixture

Graph 7 shows the ER data as the amount of oxygen in the background gas mixture was reduced and replaced with argon.

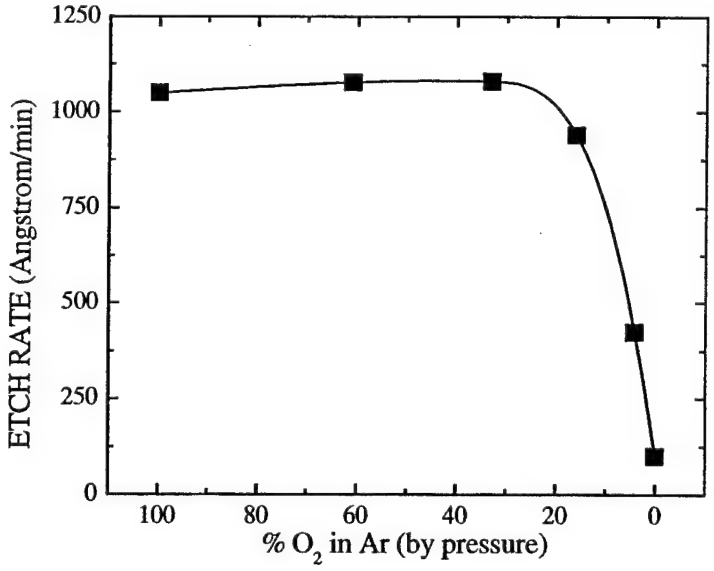

Graph 7 ER of negative resist material versus O2 percentage in plasma feedstock gas.

From this data, the etch rate remained fairly constant until the oxygen percentage dropped below 20%. The addition of argon was not exactly 1:1 with the removal of oxygen; the total pressure of the mixtures was ~ 65 mtorr, while for the pure gases, 55 mtorr of O_2 and 80 mtorr of Ar were used, respectively. At these conditions the cathode operation was very similar, with slightly higher density plasmas being formed in the pure Ar case.

4.4. Etch rate with respect to temperature

As mentioned in Section 3.2, there were two identical etching stages constructed, one equipped with water cooling lines and the other with a 300 W resistive heater element. These stages were used to adjust the substrate temperature from 0 - 200°C. With the sample temperature ranging from 0 to 90°C, a very slight increase of etch rate was seen for identical plasma exposures with 50 eV ion energies. Above 90°C, etching nearly ceased, resulting in a data set which was statistically too sparse to estimate an activation energy for the resist removal.

4.5. Etch rate with respect to fluorine addition

To look into the effect of atomic fluorine on the removal of resist material, various amounts of SF_6 were added to O_2 plasmas run in the plexiglass chamber. A makeshift 'etching stage' was made from an optical mount post and platform, aluminum, teflon and stainless steel. The stage only had rf bias capabilities and performed similar to the larger, more robust stages discussed previously. However, this stage did not couple quite as well as the previous stages. An elusive leakage current resulted in a –15 V signal when no rf was applied to the stage. Hence, -50 V bias voltages were achieved with much lower peak-to-peak rf voltages (44-50 V) and much larger mean rf current measurements. Table VII gives the experimental conditions and resultant etch rates. Cathode operation was held at –2kV/5ms pulses/20 Hz repetition rate and rf bias voltage was kept constant at –50 V.

Table VII Conditions and ER for O_2/SF_6 mixtures

PARTIAL PRESSURE (mtorr)						ER
O_2	SF_6	% SF_6	V^{rf}_{pp}(V)	I^{rf}_{mean} (mA)	I^{rf}_{pp}(A)	(nm/min)
53	0	0	50	26	1.71	77
52.7	0.6	1	52	24	1.77	88
52.8	2.1	4	44	24	1.47	56

5. RESULTS AND DISCUSSION

5.1. Cathode Operation and External Sensors

Once the issues listed in Sections 3.1 were addressed, cathode operation went smoothly and became virtually maintenance-free. The fundamental keys were (1) upgrading *all* of the electronic components for larger duty cycles (as demonstrated) and (2) careful cleaning of the cathode with lint-free cloths and methanol. As alluded to in Section 3.1.1 and mentioned in a Section 3.3.3 footnote, the electron-tube modulator was abandoned after fundamental operating issues could not be resolved.

The effects of the power supply upgrades have little bearing on the external sensor measurements. The problems associated with external sensor measurements were the dc levels and magnitudes, not the temporal response or signal droop during the high voltage pulse. Most troublesome was the behavior of the 'beam dump' monitor, which showed tremendous attenuation with duty factor, while the other measurements stayed fairly constant. This may be due to the fact that the large plate being used as the collector is a very large capacitor, which could not respond to the low signals accurately enough. The identical slotted anode monitor behaved much more realistically, possibly because it was exposed to the high field hollow cathode region on one side. In spite of the widespread use of these external sensors, it was reassuring to see in Graph 1 the minimal effects on the plasma as measured by an in situ probe measurement. The stability of the Langmuir probe measurement is only paralleled by the external voltage divider and is therefore considered the only external sensor truly indicative to changes in plasma behavior. The attenuation of the probe measurements with duty factor after the power supply upgrades may actually be due to gas heating effects, which has not yet been investigated.

5.2. Stage Characteristics

5.2.1. Stage as a probe test

The data from the floating stage (Table IV) was physically unrealistic but is included here for completeness. Given the massiveness of the stage and wiring to accommodate a robust etching environment, using the stage in such a configuration presents a number of problems, most importantly being the large capacitive load it represents. Temporal dependencies of these signals were also very unphysical and strongly tied to the

repetition rate of the plasma. The ion saturation measurements taken with the biased stage are qualitatively quite good. During the pulse, variation of signal level can be seen in Graph 2, although the signals do indeed appear to be leveling out. These temporal variations may also be due to the character of the stage-plasma interaction or merely the stage design and not necessarily indicative of the plasma. The change in collected current with respect to V_{bias} is reasonable, given the present conditions.[i] The important fact to note here is the agreement between these two [non-ideal] measurements rather than the actual values. Furthermore, the current densities measured with the stage are fairly independent of cathode repetition rate, which agrees with data in previous section. The Pearson coil in the pick-off box (Graph 2b) does show problems at these pulse lengths, shown by the baseline overshoot and decay at the end of the pulse in Graph 2b.

5.2.2. Rf biasing of stage

Most of stage developments mentioned previously were on-the-fly attempts to improve the stage performance. The measurements given in Graphs 3 and 4 are illustrative examples of plasma-stage interactions, to demonstrate the secondary discharge effect. Graph 5 on the other hand shows further deleterious effects of the ex situ anode sensors. Since ions cannot respond to high frequency fields, changes in these signals can only be due to electron currents, from the plasma or beam. Furthermore, the beam electrons should not be affected by the small rf voltages applied to the stage. Thus, the anodes, which are believed to be measures of the electron beam, should be immune to any significant changes with the application of rf to the stage. However, both measurements go to zero with the rf signal applied to the stage, which implies all electron currents have ceased. Since the plasma is still visible and the other plasma sensors are unchanged in terms of their dc signal levels, it can be reasonably assumed that the electron beam and plasma are unchanged, and these measured phenomena are at best unphysical and should not be relied on, even as qualitative diagnostic.

[i] Standard Langmuir probe theory (OML) implies that there should be minimal change in ion saturation current with probe bias. This is because most perturbations are due to the expanding sheath and effective area with a probe as the bias voltage is increased. From the geometry, the effective area of a planar probe

5.3. Etching

5.3.1. Stage Diagnostics

Although the signals measured by the rf pick-off box are not necessarily accurate with respect to the signal at the stage surface, but they serve as guides for coupling to the plasma and day-to-day reproducibility. The voltage readings in Table VI are comparable to data seen in the scientific literature for coupling to a high-density plasma source; the peak-to-peak rf voltage is approximately twice the mean or bias voltage.[i] The rf currents measured by the Pearson coil are somewhat puzzling; the small value of the mean (bias) current is reasonable but the peak-to-peak rf currents seem extremely large. Obviously, these currents are necessary to achieve the required peak-to-peak voltages which in turn provide the bias voltage. Typically, these rf currents are not reported in the literature, so a direct comparison with other etching sources is not readily available. Using typical analyses from Leiberman and Lichtenberg[17] on capacitive discharges can be somewhat misleading as the equations tend to idealize the actual experimental situation. They show that in capacitive discharges the dc voltage on the powered electrode is nearly the same as the applied rf voltage at low pressures, because the sheath drop is small. As the pressure increases to 100 mtorr, the dc voltage at the electrode is less than the applied rf voltage, due to the significant rf voltage drop across the sheath. This general description is useful in determining the degree of capacitive discharge vs capacitive coupling of the stage to the plasma. If the dc voltage measured on the stage is comparable to the applied rf voltage, then the capacitive discharge component of the etching stage may be dominant. This is encouraging when the data in Table VI is considered but disconcerting when reviewing the data from the O_2/SF_6 etches carried out in the plexiglass chamber. Even with pure O_2, it appears that the stage was not well coupled to LAPPS, but behaving more like a separate capacitive discharge.

There are a number of literature references which deal with the subject of rf biasing electrodes,[24] and a practical approach is to focus on results which most resemble the experimental setup used in these experiments. In plasma etching reactors, the bias

---

does not increase as the sheath grows. More importantly in this case is the large area of the 'probe' and the fact that the stage cannot be considered as non-perturbing to the plasma.

produced on the etching stage is given by[25] the power applied the electrode (P) divided by the plasma's ion current density and the area of the electrode. The power should be calculated by $I \times V \times \cos\varphi$, measuring the rf current (I), rf voltage (V) and the phase between them (φ), which can be non-trivial. Typically, the power is read off of the meter on the rf supply unit. Hence, there is no figure of merit for the coupling of the stage to the plasma source – applying this equation does not guarantee that the applied rf power is only increasing the energy of the incident plasma ions and not providing an additional ionization source. It has actually been shown by a group at Lam Research Corporation[26] that the ion energy can indeed be related to the peak-to-peak rf voltage (V_{pp}). Experimentally, an external voltage probe was used to correlate the sheath potential and peak rf voltage ($V_{pp}/2$). The sheath potential was determined by the sum of the plasma potential and dc bias induced on the stage, measured by an internal Langmuir probe and an external voltage probe, respectively. The correlation between the sheath voltage (i.e. ion energy) and peak rf voltage was shown to be nearly linear and unity, especially at lower applied voltages. The applied rf power on the other hand consistently showed erroneous results and was deemed an inaccurate process control quantity. Also in this work, photoresist etch rates were shown to be basically linear with the applied rf voltage. In the Lam Group's plasma source (an ICP) the plasma potential was non-negligible (~ 15V) and was included in the sheath voltage calculation whereas in LAPPS the plasma potentials are < 3 V and have not been included in the reference to ion energies or sheath voltages. Otherwise, the measurement techniques are completely analogous and in agreement with effective capacitive coupling of a stage to a high density plasma source.

5.3.2. Photoresist Removal; Ion-Driven Processes

As mentioned previously, although photoresist is generally polymeric, the specific chemical composition determines the reactivity and therefore etching characteristics. Designations of i-line, g-line, etc... refer to various UV exposure wavelengths, not necessarily a chemical composition. With a "positive" resist, UV light (or x-rays or e-beam) breaks apart chain linkages, allowing the exposed areas to be washed away with

[i] It should be noted that this relationship was typical in argon and oxygen containing plasmas used in this resist etching study, but not strictly followed in other experiments using a more crudely constructed stage with SF_6 in the gas mixtures.

appropriate developers. "Negative" resist reacts in an opposite manner, cross linking with UV exposure and then washing away the unexposed material with appropriate developers. There are limited types of negative resists, but quite a few types of positive resist. The following is a listing of typical resist materials[27] along with their general characteristics and uses in the semiconductor industry. Table VIII summarizes this listing and Figure 5 provides a chemical structure for the basic structures where applicable.

Table VIII Details of some photoresist materials.

RESIST TYPE[i]	CHEMICAL NAME	APPLICATION
PMMA	Poly methyl methacrylate; (plexiglass)	Single-component positive resist; Used in e-beam lithography, but also x-ray and DUV; not as resistant as novolacs
PMGI	Polymethylglutarimide	Positive resist; will not intermix with other resists; lift-off resist (LOR) with high thermal stability
NOVOLAC	Diazonaphthoquinone (DNQ) novolac resin	Two-component positive resist: photoactive portion (DNQ) in a novolac resin. Recent favorite (i-line, g-line) because of high resolution and thermal stability; all lithographies;
NEGATIVE	Cyclized bis(arylazide) isoprene; (natural rubber)	Negative resist; rubber matrix containing sensitizer

[i] Many more single-component polymers, polyimides and chemically amplified resists (for DUV) are not mentioned.

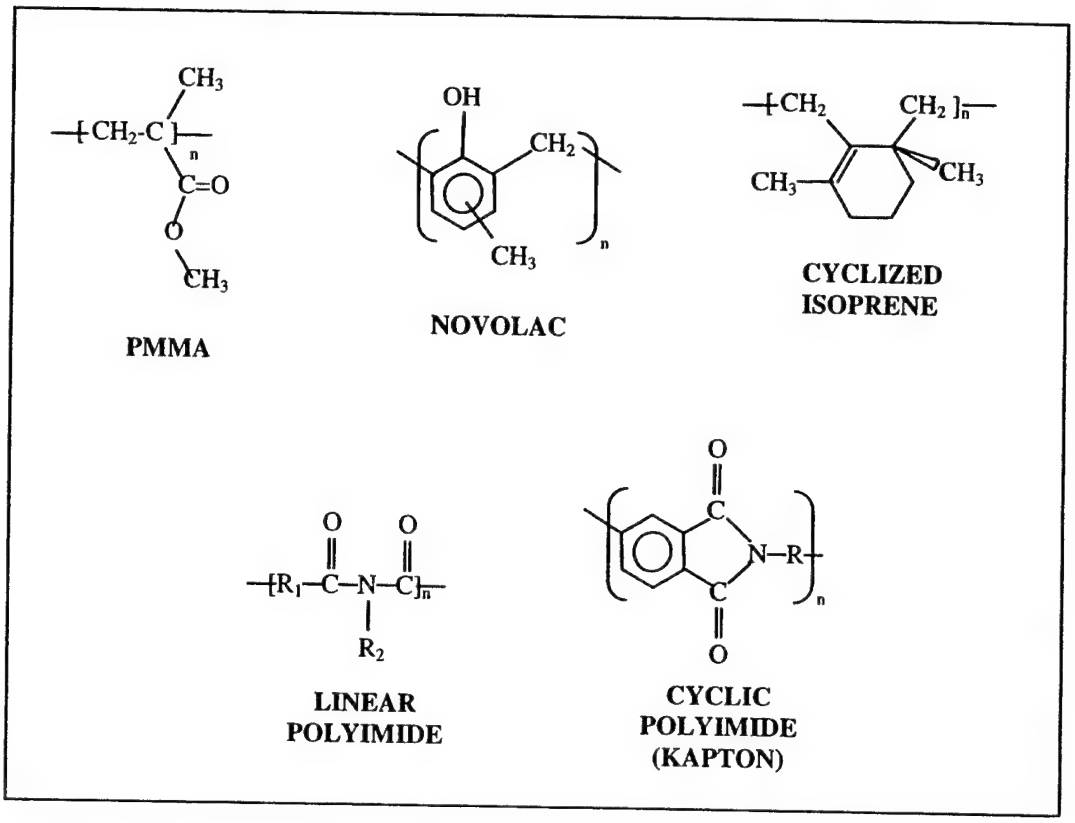

Figure 5 Chemical structures of some of the polymer materials discussed in the text

The dry chemical etch of resist materials generally relies on the desorption of carbon monoxide (CO) from the surface. While this may be fairly intuitive, the chemical composition of the actual polymer causes very different removal mechanisms. The main removal mechanism appears to be random chain scission of the polymer, which proceeds through singly-bonded carbon atoms and is proportional to the oxygen atom concentration.[28] Unsaturated (multiply-bonded) carbon atoms must first become saturated before the attack of atomic oxygen is effective in breaking the polymer backbone. Similarly, polymer structures with aromatic structures (benzene rings) are more etch resistant than non-aromatic polymers. Carbon atoms already bonded to oxygen atoms (C=O or C-O) however can more easily form CO under ion bombardment. Thus, in an oxygen deficient environment, these structures have higher sputtering yields than compounds containing fully saturated structures. The rate-determining step for resist removal then becomes the removal (sputtering) of the carbon-rich surface.

From the data shown in Graphs 6 and 7, etching of the resist material in LAPPS is strongly an ion-driven process. The direct correlation between ion energy and material removal shows that some ion energy is in fact necessary to remove material, an effect which is not necessarily true in other plasma sources. Many other plasma sources focus on the flux of atomic oxygen to the surface for material removal and do not consider the ion energy, or regard ion energy as an uncontrollable process and attempt to remove them.

In a conventional plasma source, plasma potentials from 10-100 volts are easily seen. This means that even with a grounded stage, ion energies of 10-100 eV are still impinging on the surface. In contrast, plasma potentials in LAPPS are 1-5 V in molecular gases, so initial ion energies are greatly reduced. Furthermore, from Graph 6, resist removal is not automatic (exothermic) in the presence of atomic oxygen since the ER drops to nearly zero with no bias energy. Without some sort of additional activation (ion energy, temperature), desorption of volatile etch species does not progress with measurable rates. Because of the general chemical structure of the negative resist, which is a very stable cyclic olefin, it is not surprising that additional ion energy is needed when ion energies are small, as in LAPPS. (See Section 5.3.3)

Graph 7 shows that the plasma source is not limited in neutral flux, as the etch rate remains constant as the feedstock gas source of atomic oxygen is reduced. Not until the molecular gas percentage goes to below 20% does the etch rate begin to drop. Prior to that concentration, it would be reasonable to assume that the dominant reactive species is atomic oxygen and the ion species is irrelevant; argon ions promote etching as well as oxygen ions. At first this is surprising since mass spectral data has shown that the dominant ion flux is atomic, however the dominant flux to the surface is molecular (feedstock) gas, followed by atomic neutrals and then ions. Additional support of the ion-driven resist removal in LAPPS is from the fact that there was no duty factor dependence of the ER. Some previous studies considered the molecular feedstock gas as a prime etchant which is clearly not the case in this work. Any exposed surface would indeed be active, yet no additional material removal was seen at very low duty factors. This mechanism can be discounted as a reasonable pathway for material removal in LAPPS.

The results of the via residue removal in Figure 4 show the promise of submicron feature evolution in an otherwise isotropic process. While the chromium masked samples (Figure 3) did not provide an appropriate mask for even 2 micron features, these samples provided a much more rigorous test for process anisotropy. With only very fine (50 nm) residues in small feature sizes, any process isotropy would quickly destroy the feature profile. Instead, a clean removal of the residuals left behind by a standard industrial ashing process was seen, leaving the via structure in tact. The graphitization at higher ion energies has also been seen by others[29] and apparently shows up in this sample due to the delicate structures. This is a prime example of the ion energy control and damage-free etching possibilities with electron beam produced plasmas.

Two possible phenomena should also be considered: a secondary discharge generated by the applied rf field and an unclean initial surface. The possibility of an unclean initial surface has not been fully investigated. Basically, such a mechanism implies that the [applied] external activation would only be necessary until the first five monolayers or so are removed before a clean, more reactive surface is exposed. This phenomena would manifest itself such that there would be (at least) two separate etch rates; one for the initial surface and another for the more reactive clean surface. However, the samples used in these studies were exposed to the plasma for various times and the evolution of two separate etch rates should have been apparent. The issue of a secondary discharge really resides in the coupling of the rf power to the stage, which is similar to any other plasma source. While the rf power was coupled in a reasonable way to maximize ion energies, the possibility of an rf-plasma component can not be completely ruled out, except to compare the results to a purely capacitively-driven rf system. The linear scaling of rf power and voltages does imply a strong coupling to the primary LAPPS plasma; typical capacitive discharges do not show such linear dependencies between rf voltages and bias voltage levels. Also, capacitive discharges tend to have higher discharge currents than those seen here. Thus, these issues are not considered to be dominant contributions in these experiments.

5.3.3. PR Removal; Surface Chemistry

The changes in resist removal with surface temperature was unexpected. The purpose of these particular studies was to apply the Arrhenius equation (etch rate ~ exp(-E_a/kT)) to determine an activation energy for the process. However, material removal ceased above 90 °C. It has been known that polymers (such as photoresist) have glass transition temperatures (T_g) at these temperatures, however the activation energy should increase above T_g, not go to zero. At temperatures[30] above T_g, viscous flow is possible and therefore polymer chain segments become mobile. Commercial ashing tools take advantage of this effect, incorporating rapid sample heating as part of their process. As the temperature decreases to T_g, this molecular motion decreases until all motion stops at T_g. At which point, the polymer has characteristics of glass. If T_g is above room temperature, the polymer is considered a glass; if T_g is below room temperature, the polymer is considered a rubber. For example, E_a for the PMMA resist has been shown[31] to be 3.1 to 6.5 kcal/mole below T_g (104 °C) and 9.7 kcal/mole above T_g. For the cyclic isoprene resist used in these experiments, it is conceivable that the rubber had undergone a sort of vulcanization process at the higher temperatures, making it highly resistant to the dry process. To be sure the resist did not merely flow at the higher temperature, a sample was etched at room temperature and then heated at 140-170°C for two hours under an O_2 atmosphere. The etch rate for this sample was the same as previous room temperature etches, thereby showing that the resist did not flow upon heating in the earlier experiments. For the present study, additional tests are needed (1) at various ion energies and (2) with different resist materials to further understand the observed effect.

The addition of fluorine-containing species has been used to enhance resist stripping rates on oxygen plasmas.[32] This is because F atoms produce reactive sites on the polymer backbone. Specifically, F atoms abstract hydrogen from saturated aliphatic chains (—CH_2—CH_2—) leaving radical carbon sites (—$\dot{C}H$—CH_2—) which are highly susceptible to oxidation. These sites then rapidly undergo[i] chain scission as discussed previously. Atomic fluorine will also attack double-bonded (unsaturated) carbon chains (—C=C—) reducing them to single bonds with a highly reactive radical site (—$\dot{C}$—CF—),

[i] The energy liberated when fluorine abstracts hydrogen can cleave the adjacent carbon-carbon bond. This is assumed to be the primary degradation mechanism in plasmas containing high concentrations of fluorine.

although highly saturated molecules are more susceptible to atomic F attack than the unsaturated polymer chains. From the data in Table VII, the increase of ER from 77 nm/min in the pure O_2 case to 88 nm/min with a trace of SF_6 added supports the mechanism of F atom addition to the unsaturated double bond in the cyclized isoprene molecule.[i] The observed small effect on etch rate can be attributed to the cyclic structure of the monomer which further enhances the stability of the olefinic (double) bond by delocalizing the bond character, making the molecule less reactive to chemical attack. Steric effects (how well atoms and molecules can physically fit together to undergo a chemical reaction) can also play a huge role here as well. When the SF_6 concentration was increased to 5%, deposition of sulfur-containing films became problematic, as the ER decreased rapidly. These films are not readily removed at these diminished ion energies.

Another effect associated with fluorine addition to oxygen plasmas is an increase of atomic oxygen density. This is attributed to (1) the lowering of the O wall recombination rate by F_2 and (2) halocarbon gases changing the plasma electron distribution function to favor O production. Given the overall LAPPS geometry and the fact that SF_6 was used as the fluorine source, neither of these mechanisms were considered.

6. SUMMARY

A 22 x 40 x 1cm^3 electron-beam produced plasma sheet was used to remove semiconductor grade [negative] photoresist material. A pulsed hollow cathode source operated at 2 keV in a uniform 165 Gauss magnetic field was used to supply the e-beam for these plasmas. Gas compositions primarily consisted of oxygen at 55 mtorr, which typically had plasma densities of 10^{11} cm^{-3}, electron temperatures ~ 0.5 eV and plasma potentials < 3 V. Many system upgrades were necessary to achieve reproducible, robust etching conditions, with *in situ* Langmuir probe measurements being used as the internal standard.

[i] The fact that the ER is low compared to the previous data is due to the poor coupling of the rf to the stage, mentioned in Section 4.5. It is still reasonable to compare the relative changes in the ERs, however.

Strong dependencies of etch rate on ion energies controlled by an external rf bias were seen. Specifically, etch rates increased nearly linearly from 50 to 225 nm/min as ion energies were increased from 25 to 100 eV. Anisotropy of patterned features also increased with ion energy, with good pattern transfer seen above 50 eV. Neutral atomic fluxes appear to be abundant in this plasma source, as plasma feedstock gas was replaced with argon. Etch rates remained roughly constant until the oxygen concentration fell to 20% of the feedstock gas. Addition of sulfur hexafluoride to produce atomic fluorine atoms and enhance the resist etch rate showed a small increase (~14%) in etch rate while increasing the substrate temperature completely ceased plasma-surface interactions. Both of these effects are believed to be the result of the specific chemistry associated with the negative photoresist material (cyclized isoprene) used and require additional experiments to test these hypotheses.

7. CONCLUSION

The LAPPS has demonstrated a high degree of control in anisotropically modifying negative photoresist material. A very strong ion energy dependence was shown, implying that the plasma source (1) supplies an abundance of free radical oxygen atoms and (2) additional energy is needed by the plasma ions to stimulate desorption of volatile species, even in a fairly reactive surface process as organic material removal.

ACKNOWLEDGEMENTS

A significant portion of this work could not have been completed without the technical support of Mr. Robert Lanham and Tony Noll. The helpful conversations with Dr. John Hallock of Axcelis Technologies (Rockville, MD) were greatly appreciated as well as the via samples and their ex situ analyses. This research was supported by the Office of Naval Research.

APPENDIX A

Additional literature references on resist or polymer removal:

Gokan, Ohnishi & Saigo, "Oxygen Ion-Beam Etch Resistance of Metal-Free and Organosilicon Resist Materials," *Microelectronic Engineering* **1**, 251 (1983) and Gokan, Itoh & Esho, "Oxygen Ion Beam Etching for Pattern Transfer," *JVST B* **2**, 34 (84). In these papers, and ion beam was used to 'etch' resist material. The etch rate increased with pressure and ion energy, although source dependence on these parameters is not presented. All pressures were sub-millitorr due to source. Papers point out that –C-O- structures may be readily desorbed as CO from the energy imparted by the ions. Typically used ion energies ~500 eV. Etch rate was 100-200 nm/min depending on conditions, with 200 eV ions and ~ 400 nm/min with 500 eV ions.

Cook & Benson, "Application of EPR Spectroscopy to Oxidative Removal of Organic Materials," *J. Electrochem. Soc.* **130**, 2459 (1983).

Pelletier, Arnal & Joubert, "Etching Mechanisms of Polymers in O_2 Microwave Multipolar Plasmas," *Appl. Phys. Lett.* **53**, 1914 (1988).

"Introduction to Plasma Chemistry: Oxygen Plasma Etching of Resists," D. L. Flamm in Plasma Etching: An Introduction, D. M. Manos and D. L Flamm, eds. (San Diego: Academic Press, 1989) pp. 167.

Baggerman, Collart & Visser, "Reaction Kinetics of CH Radicals during Etching of Polymers in Argon and Oxygen RF Plasmas," *J. Appl. Phys.* **71**, 5789 (1992).

Zeuner & Meichsner, "Ion Kinetic Aspects of Plasma Chemical Deposition of PMMA Films," *Vacuum* **46**, 27 (1995).

Doemling, Rueger, Oehrlein & Cook, "Photoresist Erosion Studied in an Inductively Coupled Plasma Reactor Employing CH_3F," *JVST B* **16**, 1998 (1998).

APPENDIX B

Schematic diagrams of IGBT[7] and E-tube[33] pulser units used in LAPPS operation.

Figure 6 Schematic of IGBT pulser unit from Reference 7.

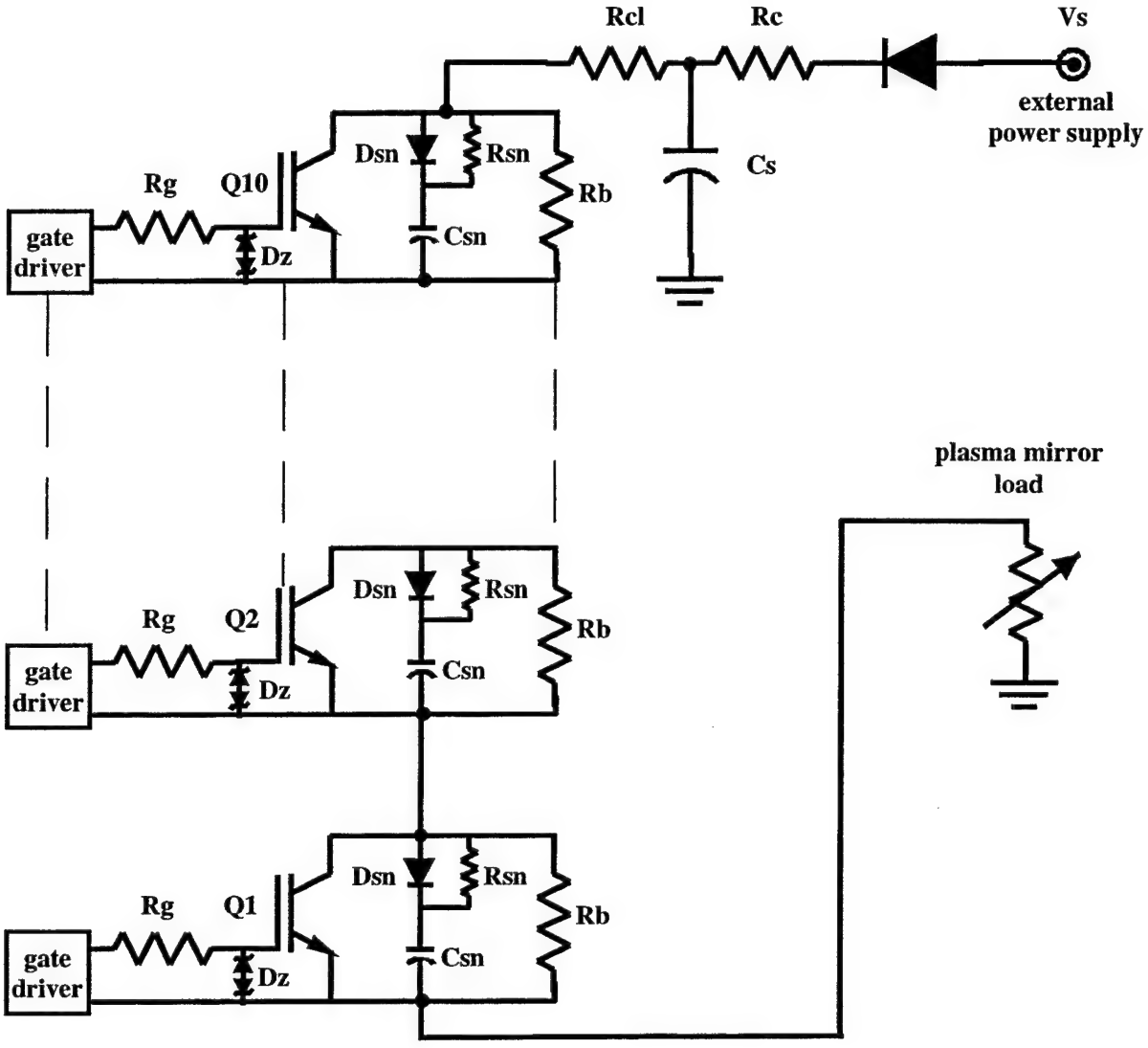

Figure 7 Electron tube pulser unit constructed to run hollow cathode

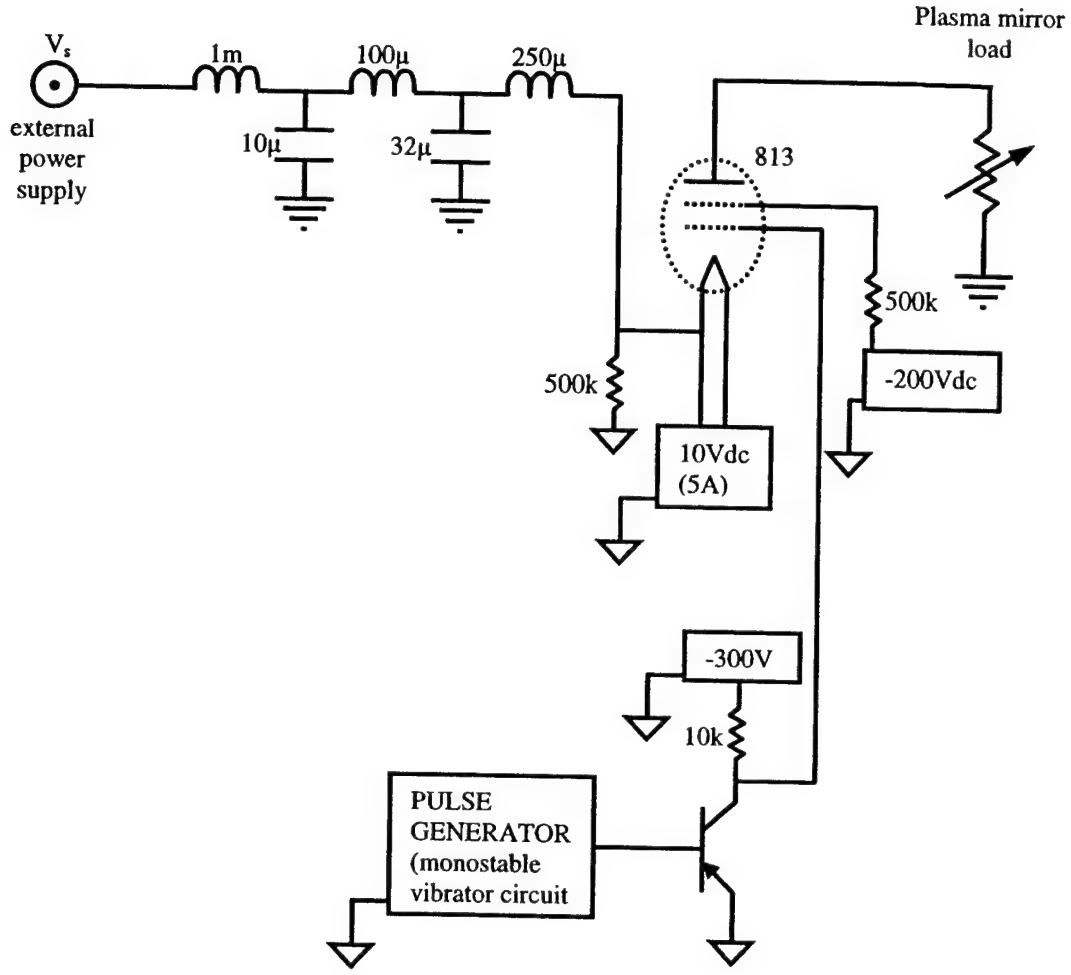

APPENDIX C

Parts drawings for etching stage. All units are in inches.

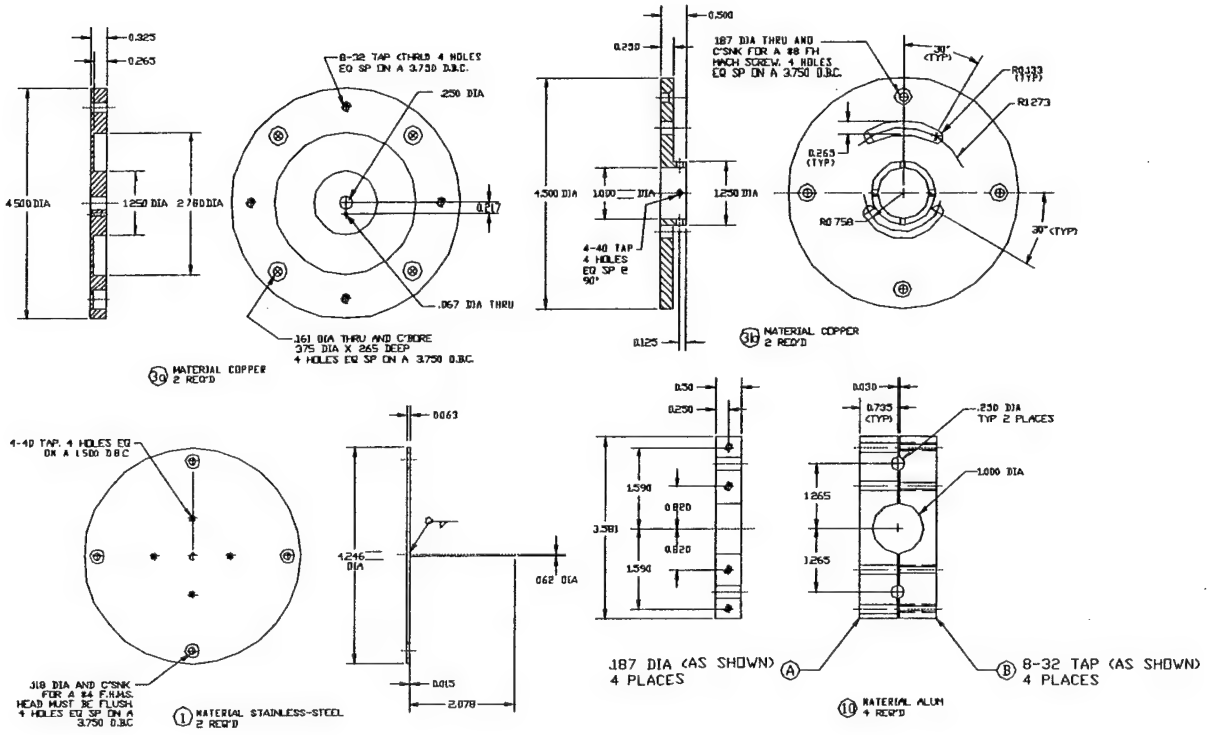

Figure 8 Metal pieces for head of etching stage assembly. All dimensions are in inches.

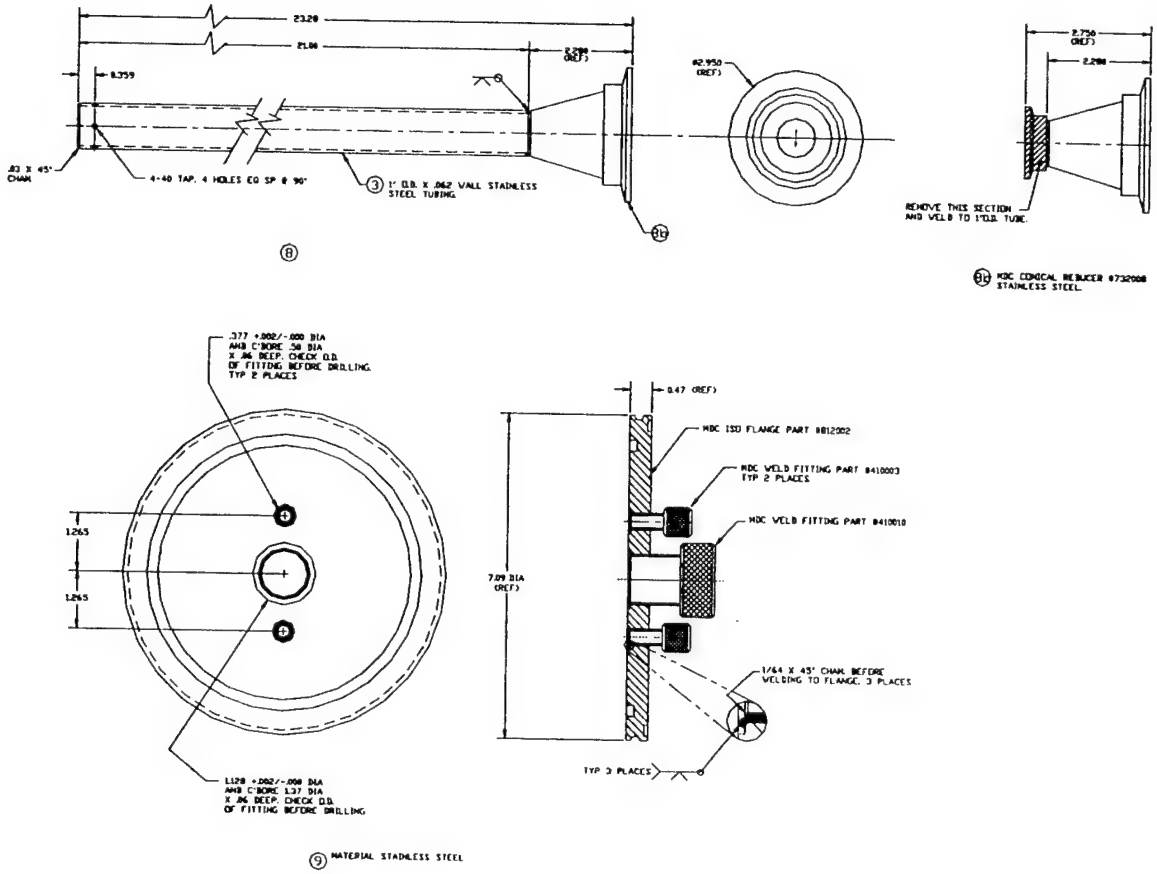

Figure 9 Shaft and mounting flange for etching stage. All dimensions are in inches.

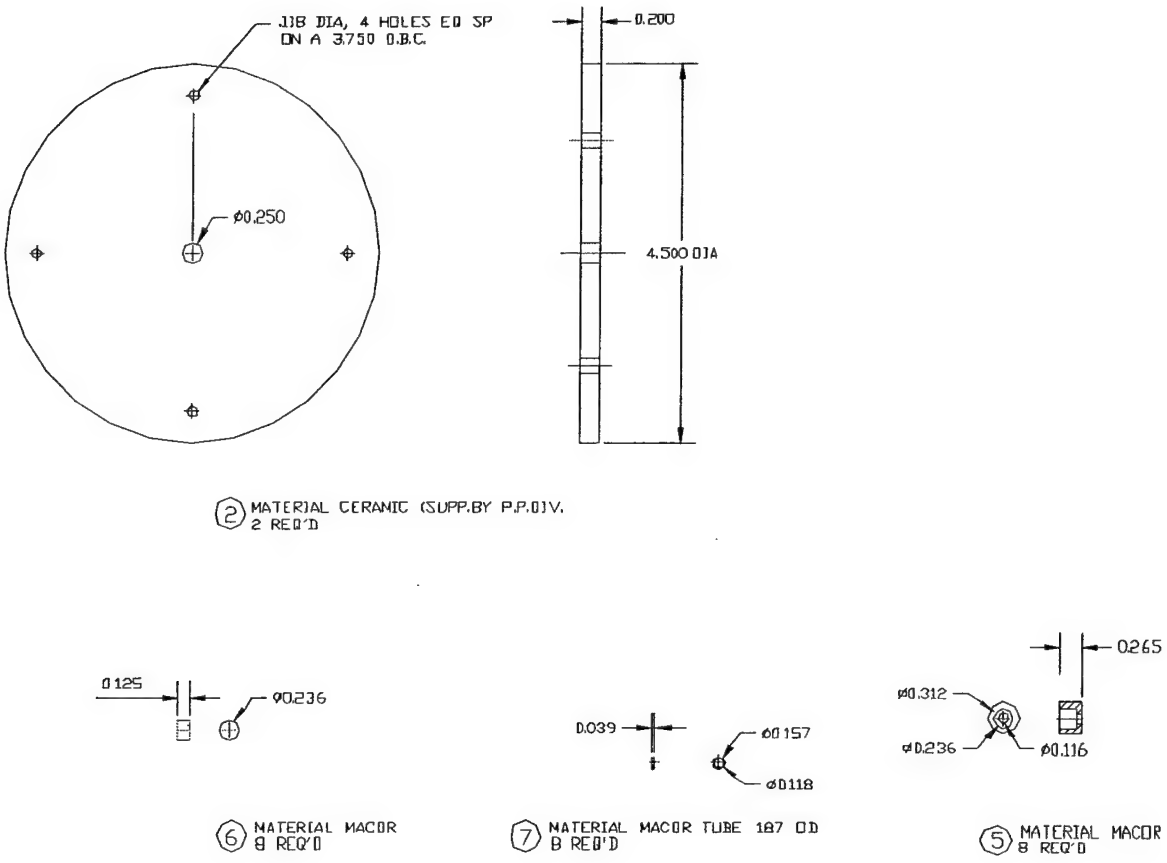

Figure 10 Ceramic pieces for etching stage assembly. All dimensions are in inches. Recess in part number 2 for front electrode not shown in drawing.

APPENDIX D
Detailed information of individual etches

BASICS

SAMPLE #	DATE RUN	DUTY FACTOR (%)	POSITION (mm from beam edge)	GAS PRESSURE	PROCESS TIME (min)	Vrfidcb (V)	ETCH RATE (nm/min)	COMMENTS
DL10-59-A	02/01/01	10	8	55mT O2	4.5		>222	beginning of new samples; cathode 'droop' problem
DL10-61-B	02/01/01	10	8	55 mT O2	3		80	still looking at cathode droop
DL10-63-C	02/02/01	10	8	55mT O2	3		125	temporarily applied very high biases to stage
DL10-64-D	02/02/01	10	8	55mT O2	6		36	
DL10-65-E	02/07/01	10	8	55mT O2	2		220	
DL10-66-G	02/07/01	10	8	55mT O2	2	-16	115	rf only
DL10-67-H	02/08/01	10	8	55mT O2	4	n/a	none	LAPPS only
DL10-68-J	02/13/01	10	8	55mT O2	3	~+1	none	LAPPS only
DL10-72-K	02/14/01	10	8	55mT O2	3	~+1.8	<28	rf only
DL10-76-L	02/15/01	10	8	55mT O2	3	~+0.17	~0; surface looks like DL10-72-K sample	rerun of rf only condition to supercede DL10-63/66 runs
DL10-88-P	03/30/01	10	8	55mT O2	15	-100	purposely blew thru sample	Check of process with improved electronics and base pressure
[illegible]								
DL10-92-O	04/02/01		8	55mT O2	3	-50	133	power failure during run; second SEM look not any better - SAMPLE SHOULDBE RERUN
DL10-95-S	07/20/01		8	55mT O2	3	-50	104.3	duty factor dependence run at otherwise std conditions; second look in LEOS better
DL10-97-T	07/23/01	10	8	25mT O2	3	-50	~33	chamber pressure dependence test; very little material removed; later measured ER~57nm/min via LEOS
[illegible]								
DL10-100-V	08/14/01	10	8		8	-50	58	rerun of DL10-97 for longer time
DL10-102-W	08/15/01	10		55mT O2	8	-50	75	rerun of DL10-98 for a longer time; accidentally re-started etch
DL10-104-X	09/07/01		8	55mT O2	3.6	-50	104	good run over very long time (6hrs of lab time)
DL10-110-Y	09/10/01		8	55mT O2	3.5	-50	85.2	good run ; no problems; second look in LEOS gave better etch depth
DL10-113-Z	10/16/01	10	8		5.3	-50	108	good run; no problems
DL10-118-AA	10/16/01	10	8		5.3	-50	94	good run; no problems
DL10-128-BB	10/24/01	10	8		6	-50	<11	good run; problems
DL10-130-CC	10/26/01	10	8		6	-50		good run; no probs
DL15-125-C	06/28/02	10	8		6	-50		good run; no probs
DL15-134-D	07/16/02	10	8		6	-50		good run; no probs
DL10-131-DD	11/01/01		8	55mT O2	6	-50		
DL10-140-FF	11/08/01		8	55mT O2	7.1	-50	109	good run; no problems
DL10-141-GG	11/09/01		8	55mT O2	6.2	-50	137	good run; initially tstarted to do 100Hz run, but couldn't
DL10-142-HH	11/13/01		8	55mT O2	6.6	-50	136	good run; no problems
DL10-144-II	11/21/01		8	55mT O2	3.69	-50	147	good run over very long time (6hrs of lab time) although exposure time was half of other's in series
DL10-146-KK	11/29/01		8	55mT O2	6	-50	95	good run w/o problems
DL10-147-JJ	11/30/01		8	55mT O2	6.2	-50	113	good run w/o problems
DL10-149-LL	12/04/01		8	55mT O2	6	-50	95	good run w/o problems
[illegible]								
DL15-7-F	12/21/01	10	8	55mT O2	6	-50	121	original run went awry; good run w/o problems
DL15-9-H	12/28/01	10	8	55mT O2	6	-50	101	good run w/o problems; sample in vacuo for some time

BASICS (cont.)

DL15-12-I	01/13/02	10	8	55mT O2	6	-50	102	good run w/o problems
DL15-13-K	01/15/02	10	8	55mT O2	6	-50	116	rerun of DL15-5-D; good run w/o problems
DL15-23-O/P	03/07/02	10	8	55mT O2	6	-50	112	rerun of DL15-11-G; no problems
DL15-25-Q/R	03/08/02	1	8	55mT O2	6	-50	113-132	rerun of DL10-151-MM at constant temperature; no problems
DL15-46-N	03/15/02	10	8	55mT O2	6	-50	99.4	82 sccm flow; no problems
DL15-48-T	03/19/02	10	8	55mT O2	6	-50	118	no problem - beginning of T dep study
DL15-50-U	03/20/02	10	8	55mT O2	6	-50	112	no problem
DL15-51-V	03/22/02	10	8	55mT O2	6	-50	115	no problem
DL15-53-W	03/25/02	10	8	55mT O2	6	-50	109	no problem
DL15-54-X	03/26/02	10	8	55mT O2	6	-50	100	no problem
DL15-55-Y	03/27/02	10	8	55mT O2	6	-50	107	no problem
DL15-59-VIAC	05/02/02	10	8	55mT O2	7.1	-50	n/a	no problem; etching of Cu vias
DL15-61-VIAD	05/03/02	10	8	55mT O2	6	-100	n/a	no problem; etching of Cu vias
DL15-65-Z	05/14/02	10	8	55mT O2	6	-50	115	higher temperature etching begins
DL15-69-B	05/14/02	20	8	55mT O2	6	-100	n/a	no problem; etching of Al vias
DL15-73-C	05/14/02	10	8	55mT O2	3	-50	n/a	no problem; etching of Al vias
DL15-79-BB	05/15/02	10	8	55mT O2	6	-50	none	higher temperature etching continues
DL15-81-CC	05/16/02	10	8	55mT O2	6	-50	none	higher temperature etching continues
DL15-86-EE	05/20/02	10	8	55mT O2	3	-50	<67	rerun of DL15-81-CC
DL15-90-FF	05/20/02	10	8	55mT O2	1.5	-50	none	rerun of DL15-79-BB
DL15-93-HH	05/21/02	10	8	55mT O2	1	-50	none	rerun of DL15-81-CC
DL15-107-II	05/23/02	10	8	55mT O2	2	-50	none	rerun of DL15-81-CC, except longer time
DL15-111-PR	05/23/02	10	8	55mT O2	2	-50	none	lower temperature
DL15-127-B	07/01/02	10	8	55mT O2	6.3	-50	77	beginning of O2/SF6 etch in plexi; no probs
DL15-129-F	07/02/02	10	8	53/0.6mT O2/SF6	6	-50	88	O2/SF6 etch in plexi; no probs
DL15-131-G	07/02/02	10	8	53/2.1mT O2/SF6	6	-50	56	O2/SF6 etch in plexi; no probs
DL15-136-H	07/18/02	10	8	55mT O2	6	-50	75	retry of DL15-127-B
DL15-146-E	08/19/02	10	8	55mT O2	6	-50	111	rf on stage twice that of LAPPS pulse
DL15-148	08/20/02	10	8	55mT O2	6	-50	106	heated sample after processing to see if resist would flow

CATHODE

SAMPLE #	CHAMBER BASE PRESSURE	Va-k (kV) applied	Voltage Divider (V)	PULSE LENGTH (ms)	REP RATE (Hz)	DUTY FACTOR (%)	LAB TIME (min)	ETCH RATE (nm/min)
DL10-59-A	2.00E-05	2		5	20	10	45	>222
DL10-61-B	1.00E-05	2		5	20	10	30	80
DL10-63-C	1.30E-05	2		5	20	10	30	125
DL10-64-D	1.50E-05	2		5	20	10	60	36
DL10-65-E	1.30E-05	2		5	20	10	20	220
DL10-66-G	1.10E-05	2		5	20	10	30	115
DL10-67-H	1.20E-05	2		5	20	10	40	none
DL10-68-J	1.70E-05	2		2	20	10	30	none
DL10-72-K	1.20E-05	2	n/m	5	20	10	30	<28
DL10-76-L	1.40E-05	n/a	n/m	5	20	10	30	~0; surface looks like DL10-72-K sample
DL10-88-P	2.00E-06	2	n/m	5	20	10	150	purposely blew thru sample
DL10-90-Q	7.50E-07	2	n/m	5	20	10	30	
DL10-92-O	1.60E-06	2	n/m	5	5	2.5	105	133
DL10-95-S	7.50E-07	2	n/m	5	10	5	60	104.3
DL10-97-T	8.00E-07	2	n/m	5	20	10	30	~33
DL10-100-V	8.00E-07	2	-23	5	20	10	80	58
DL10-102-W	7.00E-07	2	n/m	5	20	10	80	75
DL10-104-X	6.00E-07	2	-23.5	5	2	1	360	104
DL10-110-Y	5.50E-07	2	-(18-18.5)	5	100	50	7	85.2
DL10-113-Z	7.50E-07	2	-22.5	5	20	10	53	108
DL10-118-AA	8.50E-07	2	-22.4	5	20	10	53	94
DL10-128-BB	9.50E-07	2	-23	5	20	10	60	<11
DL10-130-CC	6.00E-07	2	-22	5	20	10	60	
DL15-125-C	6.00E-07	2	-(22.9-23)	5	20	10	60	
DL15-134-D	5.00E-07	2	-(22.2-22.7)	5	20	10	60	
DL10-131-DD	6.00E-07	2	-22				62	
DL10-140-FF	5.50E-07	2	-20.4	5			28.5	109
DL10-141-GG	5.50E-07	2	-22.8	5			124	137
DL10-142-HH	3.80E-07	2	-23.3	5			264	136
DL10-144-II	5.50E-07	2	-23.3	5			369	147
DL10-146-KK	5.50E-07	2	-(18-19)	5			12	95
DL10-147-JJ	5.50E-07	2	-22.8		20		155	113
DL10-149-LL	5.35E-05	2	-(21.7-21.4)		20		30	95
DL15-7-F	4.60E-07	2	-(21.5-22.2)	0.2		10	60	121
DL15-9-H	3.20E-07	2	-(22-22.3)	1		10	60	101
DL15-12-I	3.40E-07	2	-(22.3-22.7)			10	60	102
DL15-13-K	3.40E-07	2	-21.8	0.5		10	60	116
DL15-23-O/P	n/m	2	-22	2		10	60	112
DL15-25-Q/R	n/m	2	-23.4		20	1	410	113-132
DL15-46-N	5.50E-07	2	-(21.9-22.5)	2	50	10	60	99.4
DL15-48-T	4.20E-07	2	-(21.9-22.3)	2	50	10	60	118
DL15-50-U	5.00E-07	2	-22.4	2	50	10	60	112
DL15-51-V	3.00E-07	2	-(21.6-22.2)	2	50	10	60	115
DL15-53-W	3.00E-07	2	-(21.9-22.3)	2	50	10	60	109
DL15-54-X	4.00E-07	2	-(21.7-22.3)	2	50	10	60	100
DL15-55-Y	4.00E-07	2	-(22.1-22.5)	2	50	10	60	107
DL15-59-VIAC	5.00E-07	2	-(22.1-22.7)	2	50	10	71	n/a
DL15-61-VIAD	3.00E-07	2	-(22.0-22.4)	2	50	10	60	n/a
DL15-65-Z	8.00E-07	2	-(22.0-22.4)	2	50	10	60	115
DL15-69-B	5.00E-07	2	-(20.8-21.6)	2	100	20	30	n/a
DL15-73-C	5.00E-07	2	-(22.1-22.2)	2	50	10	30	n/a
DL15-79-BB	2.00E-06	2	-(21.9-22.4)	2	50	10	60	none

CATHODE (cont.)

DL15-81-CC	5.00E-07	2	-(22-22.5)	2	50	10	60	none
DL15-86-EE	3.00E-07	2	-(21.9-22.3)	2	50	10	30	<67
DL15-90-FF	2.00E-06	2	-(21.9-22.2)	2	50	10	15	none
DL15-93-HH	4.00E-07	2	-21.8	2	50	10	10	none
DL15-107-II	9.00E-07	2	-22.1	2	50	10	20	none
DL15-111-PR	2.00E-06	2	-(21.9-22.3)	2	50	10	50	none
DL15-127-B	0.00E+00	2	-(9.5-9.9)	5	20	10	63	77
DL15-129-F	0.00E+00	2	-9.5	5	20	10	60	88
DL15-131-G	0.00E+00	2	-9.5	5	20	10	60	56
DL15-136-H	0.00E+00	2	-9.5	5	20	10	60	75
DL15-146-E	5.00E-07	2	-22	2	50	10	60	111
DL15-148	5.00E-07	2	-22.4	2	50	10	60	106

RF INFO

SAMPLE #	Vpp (volts)	Ipp (amps)	Tmax
DL10-59-A	207	2.38 (50)	32
DL10-61-B	99	1.23	36
DL10-63-C	147	1.772	28
DL10-64-D	45	0.64	30
DL10-65-E	194	2.34	26
DL10-66-G	219	1.97	29
DL10-67-H	n/a	n/a	27
DL10-68-J	122	0.947	22
DL10-72-K	119	0.92	23
DL10-76-L	182	1.352	?
DL10-88-P	110	1.17	57
DL10-90-Q	90.6	1.17	27
DL10-92-O	91	1.22	34
DL10-95-S	87	2.06	26
DL10-97-T	92	2.05	23
DL10-100-V	102	2.28	31
DL10-102-W	92	2.27	40
DL10-104-X	79	2.3	47
DL10-110-Y	88	2.2	27
DL10-113-Z	80	2.2	27
DL10-118-AA	79	2.5	29
DL10-128-BB	66	2.93	30
DL10-130-CC	85	2.25	35
DL15-125-C	80	2.47	30
DL15-134-D	76.5	2.39	35
DL10-131-DD	81	2.31	35
DL10-140-FF	85	2.25	33
DL10-141-GG	80.2	2.2	45
DL10-142-HH	80.1	2.25	43
DL10-144-II	80.1	2.24	40
DL10-146-KK	88.8	3	29
DL10-147-JJ	82	2.29	38
DL10-149-LL	83	2.29	32
DL15-7-F	81.5	2.26	37
DL15-9-H	82	2.18	36
DL15-12-I	84.8	2.2	36
DL15-13-K	83	2.2	>33
DL15-23-O/P	85.3	2.14	35
DL15-25-Q/R	82.8	2.15	21
DL15-46-N	78.9	2.1	34
DL15-48-T	76.8	2.15	
DL15-50-U	77.6	2.17	
DL15-51-V	78.2	2.19	
DL15-53-W	78.4	2.11	
DL15-54-X	79.7	2.16	
DL15-55-Y	86.6	2.33	
DL15-59-VIAC	83.1	2.21	41
DL15-61-VIAD	183	4.5	23
DL15-65-Z	62.3	2.66	100
DL15-69-B	179.6	4.3	27
DL15-73-C	80.6	2.18	25
DL15-79-BB	65.3	2.71	
DL15-81-CC	77.2	2.9	
DL15-86-EE	75.3	2.86	
DL15-90-FF	77.8	2.91	
DL15-93-HH	80.2	2.96	
DL15-107-II	63.6	2.73	
DL15-111-PR	63.1	2.87	

SURFACE

SAMPLE #	SEM
DL10-59-A	removed all PR; a lot of grass; mask failed
DL10-61-B	mask OK; grassy surface
DL10-63-C	mask damaged; grassy surface
DL10-64-D	mask OK; severe mushrooming under mask;
DL10-65-E	mask stressed; good anisotropy;
DL10-66-G	good anisotropy; mottled-looking surface instead of grass; slight mushrooming under mask
DL10-67-H	no material removed
DL10-68-J	mask appears to be stressed but no material removal
DL10-72-K	surface looks barely touched; worst case scenario is 27.nm/min removal rate
DL10-76-L	surface looks barely touched;
DL10-88-P	complete removal of PR but residue still remains; severe mushrooming under mask edges
DL10-90-Q	some minor mushrooming; grass seems less severe
DL10-92-O	mask slightly stressed; severe mushrooming and surface roughening
DL10-95-S	basically same surface condition; a lot of 'cotton' on the surface
DL10-97-T	too little material removed to make intelligent statement
DL10-100-V	grass 'globules' look to be less; no exceptionally large stuff; some mushrooming
DL10-102-W	mask took a beating; grass 'globules' OK; no exceptionally large stuff; big undercutting
DL10-104-X	decent etch; slight undercut, max under mask; surface OK
DL10-110-Y	mask took a beating; decent etch; slight undercut, max under mask; surface OK
DL10-113-Z	mask took a beating; decent etch; slight undercut, max under mask; surface OK
DL10-118-AA	mask held up; good photo; slight undercut
DL10-128-BB	mask looks untouched; little if any material removal; surface still looks 'cottoney'
DL10-130-CC	LEOS showed good looking surface (no cotton); big undercutting
DL15-125-C	rinsed; measuremets skewed due to low removal
DL15-134-D	rinsed; good photos
DL10-131-DD	LEOS showed good looking surface (no cotton); big undercutting
DL10-140-FF	mask took a beating; no gold coating; LEOS showed good looking surface (no cotton); some undercutting
DL10-141-GG	mask took a beating; no gold coating; LEOS showed good looking surface (no cotton); big undercutting
DL10-142-HH	mask more damaged than previous samples; no gold coating; LEOS showed good looking surface (no cotton); appreciable undercutting
DL10-144-II	uncoated sample had problem in LEOs; mask took a beating. Undercutting at mask still present - possibly slightly less.
DL10-146-KK	uncoated sample had problem in LEOs; mask took a beating. Undercutting at mask still present.
DL10-147-JJ	uncoated sample had problems in LEOS; mask didn't hold up; undercut at mask
DL10-149-LL	uncoated sample had charging problems in LEOS; mask didn't hold up; undercutting at mask
DL15-7-F	mask didn't hold up; LEOS pics fine; undercut at mask
DL15-9-H	mask didn't hold up; LEOS pics fine; undercut at mask

SURFACE (cont.)

DL15-12-I	mask didn't hold up; LEOS pics fine; undercut at mask but sidewalls look straighter
DL15-13-K	mask didn't hold up; LEOS pics fine; undercut at mask
DL15-23-O/P	mask didn't hold up; undercut at mask; rinsed sample cleaner
DL15-25-Q/R	mask didn't hold up; undercut at mask; rinsed sample cleaner
DL15-46-N	mask didn't hold up; undercut; LEOS pics good; 46-S was rinsed sample
DL15-48-T	rinsed; mask shot; undercut badly
DL15-50-U	rinsed; mask shot; undercut badly
DL15-51-V	rinsed; mask shot; undercut
DL15-53-W	rinsed; mask shot; undercut
DL15-54-X	rinsed; mask shot; undercut
DL15-55-Y	rinsed; mask shot; profile good
DL15-59-VIAC	axcelis
DL15-61-VIAD	axcelis
DL15-65-Z	rinsed; mask shot; typical
DL15-69-B	axcelis
DL15-73-C	axcelis
DL15-79-BB	rinsed; mask shot; no material removal
DL15-81-CC	rinsed; mask shot; no material removal
DL15-86-EE	rinsed; mask shot; minimal material removal
DL15-90-FF	rinsed; mask shot; no material removal
DL15-93-HH	rinsed; mask shot; no material removal
DL15-107-II	rinsed; mask shot; no material removal
DL15-111-PR	rinsed; mask shot; no material removal
DL15-127-B	rinsed; mask shot; bad photos
DL15-129-F	rinsed; mask shot; poor anisotropy
DL15-131-G	rinsed; mask shot; poor anisotropy
DL15-136-H	rinsed; mask shot; poor anisotropy
DL15-146-E	rinsed; mask shot; poor anisotropy; can't really say it is worse than others, with rf synced to lapps only
DL15-148	rinsed; mask shot; poor anisotropy

REFERENCES

[1] D. Leonhardt, S.G. Walton, D.D. Blackwell, D.P. Murphy, R.F. Fernsler and R.A. Meger, *J. Vac. Sci. Technol. A* **19**, 1367 (2001).
[2] FusionES3I/FusionGemini ES product datasheet, 57730 Rev A (Jan. 2001) and 57940 Rev. A (May 2001) from Axcelis Technologies, Inc.
[3] Using a Novolac positive-type photoresist.
[4] R.A. Meger informal technical report from May 1, 1997 and presentation given June 1997.
[5] This and all equations are taken from the NRL Plasma Formulary unless otherwise noted.
[6] R.F. Fernsler, *"Beam Spreading,"* informal technical note, 2 February 1996.
[7] M.C. Myers, R.F. Fernsler, J.A. Gregor, J. Mathew, R.A. Meger, D.P. Murphy and R.E. Pechacek, *"Power Modulator for Broadband Agile Mirror Radar Utilizing Semiconductor Switching,"* Conference Record of the 1996 Twenty-Second International Power Modulator Symposium, (IEEE Press, NJ, 1996) pp.118.
[8] D. Leonhardt, *"Maiden Voyage of New Hollow Cathode Arrangement,"* informal technical note, 22 September 1998.
[9] See experiments in DL8-139.
[10] See experiments in DL10-45.
[11] See experiments in DL10-90 and DL10-79; latter has less data for 45 ms pulse lengths.
[12] See experiments on DL12-81.
[13] See experiments on DL12-58.
[14] See experiments on DL12-97.
[15] See experiments on DL12-107.
[16] See experiments on DL10-135.
[17] M.A. Lieberman and A.J. Lichtenberg, Principles of Plasma Discharges and Materials Processing, (Wiley, New York, 1994), pp. 340-372.
[18] See experiments on DL10-3 and DL15-21.
[19] See experiments on DL10-24.
[20] See experiments on DL10-41.
[21] See experiments on DL10-47.
[22] Photographs courtesy of John Hallock of Axcelis Technologies, Rockville, MD.
[23] See experiments on DL15-46.
[24] M.A. Sobolewski, *Phys. Rev. E* **59**, 1059 (1999) and the references therein.
[25] M.F. Doemling, N.R. Rueger, G.S. Oehrlein and J.M. Cook, *J. Vac. Sci. Technol. A* **16**, 1998 (1998).
[26] R. Patrick, S. Baldwin and N. Williams, *J. Vac. Sci. Technol. A* **18**, 405 (2000).
[27] C.G. Willson, in Introduction to Microlithography, 2nd ed., edited by L.F. Thompson, C.G. Willson and M.J. Bowden (ACS Press, Washington DC, 1994), pp.139-250.
[28] S.R. Cain, F.D. Egitto and F. Emmi, *J. Vac. Sci. Technol. A* **5**, 1578 (1987).
[29] Resist graphitization references.
[30] L.F. Thompson in Introduction to Microlithography, 2nd ed., edited by L.F. Thompson, C.G. Willson and M.J. Bowden (ACS Press, Washington, DC, 1994), pp.269-371.
[31] Harada and Katsuhiro, *J. Appl. Poly. Sci.* **26**, 1961 (1981).
[32] D.L. Flamm in Plasma Etching: An Introduction, edited by D.M. Manos and D.L Flamm (San Diego: Academic Press, 1989) p. 167.
[33] From Dwight Duncan Notebook IV.